Journal of Remote Sensing
A SCIENCE PARTNER JOURNAL

RESEARCH ARTICLE

FROM-GLC Plus 3.0: Multimodal Land Change Mapping with SAM and Dense Surface Observations

Le Yu[1,2,3*†], Zhenrong Du[4†], Xiyu Li[1], Jiatong Gu[5], Xinyue Li[4], Liheng Zhong[6], Duojiweise[7], Hui Wu[1], Qiang Zhao[1], Xiaorui Ma[4], Junqing Zheng[1], Yuanzheng Yang[8,9], Weimin Song[10,11], Pei Wang[12,13], Zhicong Zhao[12,13], Lingyun Liao[14,15], Ying Long[16], Yongguang Zhang[17,18,19], Jinbang Peng[20], Miaogen Shen[21], Tingting Li[22], Zhentao Sun[23,24,25], Yonggan Zhao[23,24,25], Chaoyang Wu[26,27], Guanghui Lin[28,29], Yong Luo[1], and Dailiang Peng[30]

[1]Department of Earth System Science, Ministry of Education Key Laboratory for Earth System Modeling, Institute for Global Change Studies, Tsinghua University, Beijing, China. [2]Ministry of Education Ecological Field Station for East Asian Migratory Birds, Beijing, China. [3] Institute of Carbon Neutrality, Tsinghua University, Beijing 100084, China. [4]School of Information and Communication Engineering, Dalian University of Technology, Dalian, China. [5]School of Land Science and Technology, China University of Geosciences, Beijing 100083, China. [6]Ant Group, Beijing 100020, China. [7]Geothermal Geological Brigade, Tibet Autonomous Region Geological and Mineral Exploration and Development Bureau, Lhasa, China. [8]Key Laboratory of Environment Change and Resources Use in Beibu Gulf, Ministry of Education, Nanning Normal University, Nanning, China. [9]Guangxi Key Laboratory of Earth Surface Processes and Intelligent Simulation, Nanning Normal University, Nanning, China. [10]Key Laboratory of Coastal Environmental Processes and Ecological Restoration, Yantai Institute of Coastal Zone Research, Chinese Academy of Sciences, Yantai, China. [11]Yellow River Delta Field Observation and Research Station of Coastal Wetland Ecosystem, Chinese Academy of Sciences, Dongying, China. [12]Department of Landscape Architecture, School of Architecture, Tsinghua University, Beijing, China. [13]Institute for National Parks, Tsinghua University, Beijing, China. [14]College of Landscape Architecture and Art, Fujian Agriculture and Forestry University, Fuzhou 350002, China. [15]Wuyishan National Park Research Institute, Fuzhou 350002, China. [16]School of Architecture and Hang Lung Center for Real Estate, Key Laboratory of Eco Planning & Green Building, Ministry of Education, Tsinghua University, Beijing, China. [17]International Institute for Earth System Sciences, Jiangsu Center for Collaborative Innovation in Geographical Information Resource Development and Application, Nanjing University, Nanjing, China. [18]Jiangsu Provincial Key Laboratory of Geographic Information Science and Technology, Key Laboratory for Land Satellite Remote Sensing Applications of Ministry of Natural Resources, School of Geography and Ocean Science, Nanjing University, Nanjing, China. [19]Jiangsu International Joint Carbon Neutrality Laboratory, Nanjing University, Nanjing, China. [20]State Key Laboratory of Efficient Utilization of Arid and Semi-Arid Arable Land in Northern China, National Hulunber Grassland Ecosystem Observation and Research Station, Institute of Agricultural Resources and Regional Planning, Chinese Academy of Agricultural Sciences, Beijing, China. [21]State Key Laboratory of Earth Surface Processes and Resource Ecology, Faculty of Geographical Science, Beijing Normal University, Beijing, China. [22]State Key Laboratory of Atmospheric Environment and Extreme Meteorology, Institute of Atmospheric Physics, Chinese Academy of Sciences, Beijing, China. [23]Department of Energy and Power Engineering, Tsinghua University, Beijing, China. [24]Beijing Engineering Research Centre for Ecological Restoration and Carbon Fixation of Saline–Alkaline and Desert Land, Beijing, China. [25]Shanxi Research Institute for Clean Energy of Tsinghua University, Shanxi, China. [26]The Key Laboratory of Land Surface Pattern and Simulation, Institute of Geographical Sciences and Natural Resources Research, Chinese Academy of Sciences, Beijing, China.

Citation: Yu L, Du Z, Li X, Gu J, Li X, Zhong L, Duojiweise , Wu H, Zhao Q, Ma X, et al. FROM-GLC Plus 3.0: Multimodal Land Change Mapping with SAM and Dense Surface Observations. *J. Remote Sens.* 2025;5:Article 0728. https://doi.org/10.34133/remotesensing.0728

Submitted 19 January 2025
Revised 21 May 2025
Accepted 17 June 2025
Published 26 August 2025

[27]University of Chinese Academy of Sciences, Beijing, China. [28]Ministry of Education Key Laboratory for Earth System Modeling, Department of Earth System Science, Tsinghua University, Beijing, China. [29]Hainan International Blue Carbon Research Center, Hainan Research Academy of Environmental Sciences, Haikou, China. [30]Aerospace Information Research Institute, Chinese Academy of Sciences, Beijing, China.

*Address correspondence to: leyu@tsinghua.edu.cn
†These authors contributed equally to this work.

Land cover mapping plays a critical role in monitoring land system changes. Despite advancements in remote sensing technologies, traditional satellite-based approaches are often constrained by cloud cover, coarse temporal resolution, and limitations in capturing fine-scale landscape dynamics, leading to gaps in continuous and real-time monitoring. Near-surface cameras offer a solution by providing high-frequency, ground-level observations that bridge temporal gaps and enhance spatial detail. Therefore, this study makes substantial contributions by pioneering the integration of near-surface camera observations with satellite imagery, addressing key challenges in imaging perspective differences and limited coverage of ground-based observations for enhanced land cover monitoring at a 30-m/10-m scale. A key innovation lies in leveraging near-surface cameras to reconstruct dense satellite data time series and capture daily land cover dynamics, addressing critical temporal gaps in traditional satellite-based approaches. The research further advances the field by implementing state-of-the-art deep learning techniques, particularly the Segment Anything Model (SAM), to achieve precise parcel-level delineation and reduce classification noise at a high-resolution (meter- and submeter level) scale. Furthermore, the framework's ability to synthesize multimodal data sources (near-surface cameras, Sentinel-1/2, and high-resolution imagery) represents a methodological breakthrough in space and surface sensor integration for real-time land cover change detection, enabling time-sensitive applications and early warning systems for land system changes.

Introduction

Land cover mapping plays a pivotal role in understanding and managing terrestrial ecosystems, offering essential insights into biodiversity conservation, climate change adaptation, and sustainable land management [1–3]. Accurate land cover maps are indispensable for modeling ecosystem services, monitoring environmental changes, and informing policy decisions [4–6]. As the Earth's surface undergoes continuous transformations due to both natural processes and human activities, the demand for high-resolution, frequently updated land cover data has become increasingly critical [7–9].

Over the past few decades, advancements in satellite remote sensing have significantly improved the spatial resolution and temporal frequency of land cover mapping [10,11]. The transition from kilometer-scale to meter-scale satellite imagery and the increasing revisit frequency of sensors such as Sentinel-2 and Landsat have enabled more detailed and timely observations [12,13]. Notable examples include MODIS Land Cover Type product (MCD12Q1) at 500-m resolution [14]; European Space Agency (ESA) Climate Change Initiative Land Cover (CCI-LC) maps at 300-m resolution [15]; the GLC_FCS30 [16], GLC_FCS30D [17], Globeland30 [18], and finer-resolution observation and monitoring of GLC (FROM-GLC) at 30-m resolution [19]; Google Dynamic World [7], ESA WorldCover [20,21], and FROM-GLC10 [22] at 10-m resolution; SinoLC-1 [23] and the EnviroAtlas One Meter-scale Urban Land Cover (MULC) [24] at 1-m resolution; and the FROM-GLC plus (FGP) at multiple spatiotemporal resolution [25]. However, a persistent gap remains in the integration of multimodal data and the inclusion of dense ground-level observations [26]. Current satellite-based approaches often face challenges in capturing abrupt land changes due to cloud cover, revisit limitations, and the lack of spatially continuous ground-truth data [27]. Additionally, existing methodologies frequently underutilize multimodal data, such as radar, optical, and near-surface observations, leaving an untapped potential for more comprehensive land cover mapping [9].

Moreover, the dual pressures of climate change and intensifying human activities have accelerated the pace of global environmental transformations [28–30]. Rapid land cover changes, such as deforestation, urban expansion, cropland management activities, and land degradation, are increasingly common and require immediate monitoring for early warning [31–33]. Traditional approaches to land cover change mapping are often constrained by their reliance on periodic satellite observations, which struggle to capture abrupt, short-term transitions. This has led to a growing demand for high-frequency monitoring systems capable of detecting and analyzing rapid land changes with improved accuracy and timeliness [34,35].

The emergence of advanced computational technologies, including supercomputing, cloud-based platforms, and near real-time remote sensing data acquisition capabilities, has created new opportunities for rapid and dynamic land cover monitoring. Examples include Dynamic World [7] and FGP 2.0 [36], both of which leverage Sentinel-2 data to provide near real-time dynamic land cover mapping at 10-m resolution, offering valuable tools for monitoring environmental transformations and supporting decision-making processes. However, since these products rely exclusively on single-source remote sensing data (e.g., Sentinel-2), their temporal density and real-time capabilities remain constrained by the inherent limitations of satellite data acquisition, such as revisit cycles. This challenge is particularly pronounced in regions with frequent cloud cover and rainfall, where consistent and continuous observations are difficult to achieve [37,38]. Additionally, validating the accuracy of dynamic mapping products remains a significant challenge. Unlike static land cover classification, which can be validated using well-established datasets, the validation of land cover changes requires capturing transient events, which are often short-lived and spatially heterogeneous. The collection of validation samples for dynamic surface changes at a global scale is inherently difficult due to the lack of spatially and temporally dense ground-truth data, making it challenging to objectively and effectively quantify the accuracy of dynamic mapping products. This limitation underscores the need for complementary ground-based observations to enhance validation efforts and improve the reliability of dynamic land cover mapping.

Recently, the rapid development and expanding deployment of near-surface cameras—ranging from phenology cameras to traffic monitoring cameras, travel cameras, and geo-tagged photos—offer unprecedented opportunities for timely and rapid land system monitoring [39–41]. These ground-level observation networks are increasingly recognized for their ability to capture localized environmental changes, providing dense, high-frequency data that complement satellite observations [41,42]. The near-surface cameras can be used for capturing abrupt land changes, such as vegetation phenological shifts and sudden landscape changes [43–45]. Furthermore, near-surface cameras provide critical ground-truth data, making them an invaluable resource for validating the accuracy of dynamic land cover mapping products [46–48]. Their capacity to operate at the parcel level further aligns with the increasing emphasis on semantic segmentation and object-based mapping, particularly in the context of high-resolution remote sensing [49]. By integrating data from near-surface cameras with multimodal satellite imagery, this approach shows the potential to address existing gaps in spatial and temporal resolution, offering a more robust framework for monitoring and validating land cover dynamics.

Given these advancements, this study proposes a novel framework that leverages near-surface cameras and multimodal data for multiple spatiotemporal resolution land cover mapping. This framework addressed challenges in combining the high-frequency observations of near-surface cameras with the wide spatial coverage of satellite remote sensing to generate daily satellite data. Consequently, the framework overcomes the limitations of traditional methods in timeliness of land cover mapping and meets the demands of monitoring abrupt land changes. The study further explores the use of advanced computer vision models, Segment Anything Model (SAM) [50], for high-resolution parcel-level segmentation, offering a flexible and scalable solution for multiscale and timely land cover mapping on demand. This approach not only improves the accuracy of land cover classifications but also provides a robust foundation for understanding and managing rapidly changing land systems in a time-sensitive manner.

The rest of this paper details the study area and datasets, including the photos collected by near-surface cameras, followed by the methodological framework of FGP 3.0, which incorporates annual land cover mapping, dense dynamic land cover monitoring, and high-resolution parcel-level classification using SAM. The experimental results and validation analysis demonstrate the effectiveness of the proposed approach in capturing land cover dynamics with improved spatial and temporal resolution. A discussion follows, highlighting the advantages, limitations, and potential improvements of the framework, along with its applications in early warning systems. Finally, the paper concludes by summarizing the key findings and outlining future research directions.

Dataset and study area

Global long-term near-surface camera networks

There are several near-surface camera networks around the globe, each with different characteristics (such as distribution and scale) (Fig. 1). The PhenoCam Network (PhenoCamN) is the largest near-surface camera network globally, focusing mainly on North America. It boasts global coverage and approximately 750 site-years of observations (https://phenocam.sr.unh.edu/webcam/) [51,52]. In addition, there are respective near-surface camera networks in other continents. The European Phenology Camera Network (EPCN) focuses on Europe and consists of ~69 sites (https://fmiprot.fmi.fi/index.php?page=EUROPHEN) [53], while the Australian Phenocam Network (APN) was established in Australia and has more than 300 sites up to now (http://phenocam.org.au/) [54]. The Phenological Eyes Network (PEN), composed of ~30 sites, is mainly distributed in Japan, with several sites in other Asian countries (http://pen.envr.tsukuba.ac.jp) [55]. Brazil Phenocam Network (also known as ePhenology network, BPN) also deploys several sites in Brazil [56,57], as well as Indian PhenoMet Network (IPN) that consists of 5 sites in India [58–62].

The global network of near-surface camera sites is not evenly distributed, with significant gaps in coverage across Asia, Africa, and Latin America. To address this disparity, we established the Near Surface Cameras Network (NSCamN), which consists of more than 100 cameras primarily focused on China (Fig. 1) [42]. NSCamN includes 2 main types of monitoring cameras. First, it incorporates traditional phenology cameras, commonly used in existing near-surface camera networks, which are manually installed and programmed to capture images at hourly intervals. Second, it integrates continuous monitoring video feeds provided by China Tower, from which a single frame is extracted every hour to generate hourly observational data. China Tower, as one of the world's largest telecom tower infrastructure providers, has expanded its services to include environmental monitoring through its extensive network of towers. Leveraging its infrastructure, China Tower supports high-resolution, real-time environmental observation, offering a valuable source of near-surface data for dynamic land cover monitoring. The integration of China Tower data highlights NSCamN's capacity to integrate diverse sources of near-surface camera data, such as traffic monitoring cameras and travel cameras, enabling the effective utilization of existing land surface observation networks across a wide range of environments. Therefore, we believe that the NSCamN can provide new observations and supplement the gaps in spatial coverage, thereby facilitating data exchange and collaborative research.

Global near-surface camera networks play a crucial role not only in providing continuous surface dynamic monitoring but also in serving as validation tools at varying temporal frequencies (Fig. 2). Here, we listed 4 different varying temporal frequencies including seasonal change, monthly change, 10-d change, and daily change. As for seasonal change, we observe the broad patterns of grassland change in a year at a site in North Dakota, USA, which highlights how plant phenology shifts across different seasons from winter (snow-covered), spring (snow-melted), to summer (lush green) and autumn (browning) (Fig. 2A). As for monthly change, Fig. 2B offers a more detailed look at how the land field transforms from bare land to plowed and then to

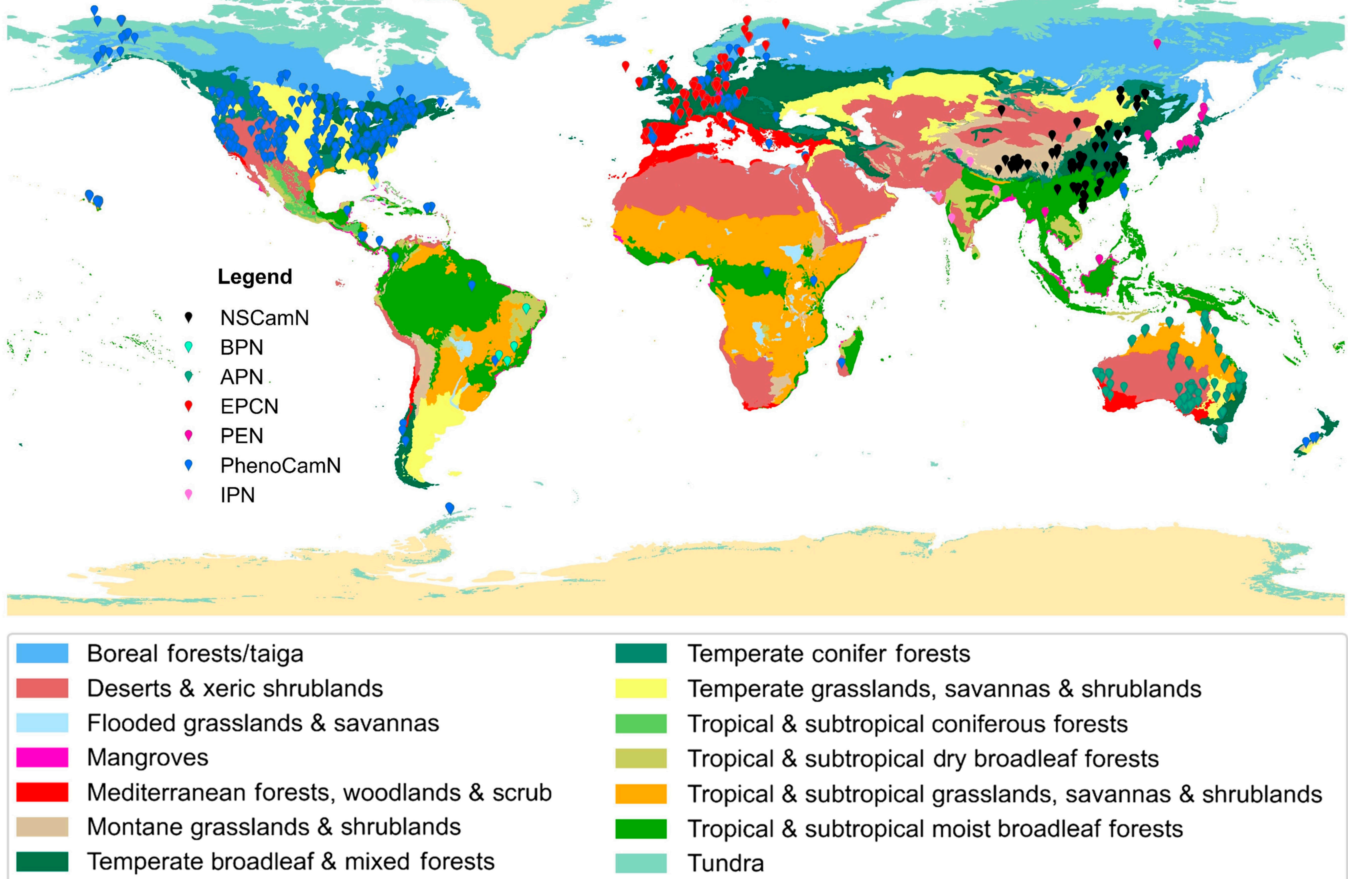

Fig. 1. Global distribution of near-surface camera networks.

flooding and vegetative over the stages of crop phenology at a rice field site in Spain. Figure 2C delves into the nuances of 10-d intervals, providing a closer look at the maize harvest dynamics occurring gradually within a month at a site in Pennsylvania, USA. Lastly, Fig. 2D showcases daily changes in rice harvest periods at a site in Arkansas, USA, which illustrates the rapid and subtle changes in vegetation that occur from 1 d to the next. These photos provide a comprehensive view of vegetation dynamics at multiple time scales.

Study area

This study selected 8 near-surface camera sites globally, with the 5° × 5° grid containing each camera site defined as the corresponding mapping study area (Fig. 3). The sites are located in Asia, Europe, North America, South America, Africa, and Oceania. The selection of study areas was based on 2 key criteria: the availability of continuous near-surface camera data for 2024, and the geographical diversity of the sites to ensure coverage of different global ecological zones and land cover types. Among the 8 selected sites, 6 are from the PhenoCamN and 2 are from NSCamN located in China. The Chinese sites include one phenology camera station and one tower station provided by China Tower.

This diverse selection of sites ensures that the study addresses a wide range of ecological conditions and land cover patterns, enabling the evaluation of the proposed land cover mapping framework. Specifically, according to the International Union for Conservation of Nature (IUCN) ecosystem typology [63], these grids encompass diverse terrestrial ecosystems, including intensive land use region in Grid a and Grid e, savanna and grassland region in Grid b, Grid f, and Grid h, shrubland and shrubby woodland region in Grid c, temperate-boreal forests and woodlands in Grid d, and tropical or subtropical forest region in Grid g.

Methods

The FGP 3.0 framework integrates multimodal data sources to achieve accurate and scalable land cover mapping based on FGP 1.0 and 2.0. The methodology consists of 3 key components: annual land cover modification, dense dynamic land cover monitoring, and high-resolution land cover classification (Fig. 4). Annual mapping combines Sentinel-2 spectral and Sentinel-1 Synthetic Aperture Radar (SAR) features with near-surface camera observations, using a spatial matching algorithm to reconstruct dense daily Sentinel-2 normalized difference vegetation index (NDVI) time series and improve classification accuracy. Dynamic mapping extends this framework by incorporating near-surface camera dense observations to detect continuous and abrupt land cover changes at a daily scale, addressing the delay and limitations of satellite-only products. High-resolution mapping leverages SAM to perform parcel-level segmentation and refine land cover classifications, reducing noise and enhancing spatial precision. Furthermore, parcel-level monitoring enables

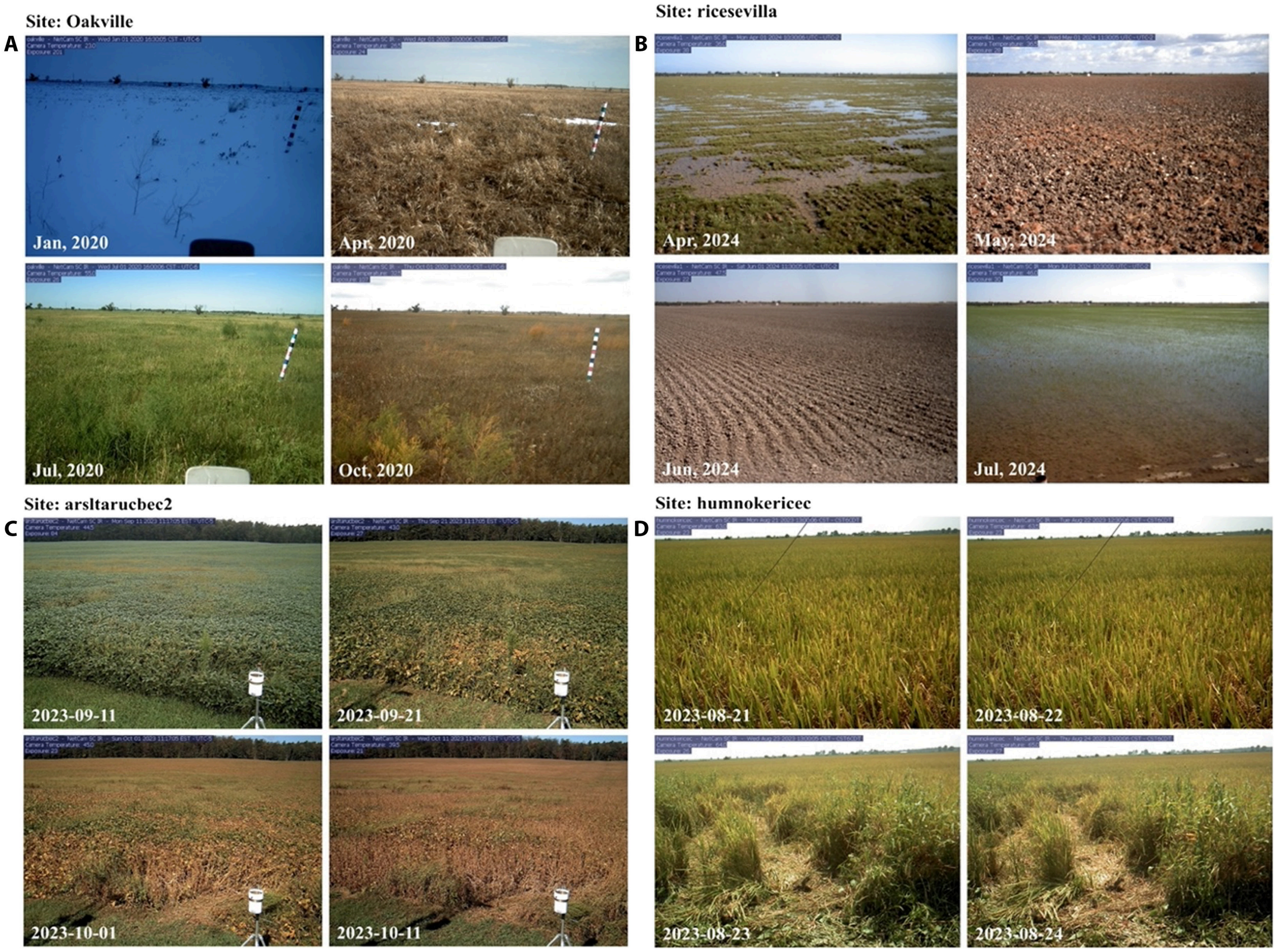

Fig. 2. PhenoCam photos in different time frequency change. (A) Seasonal change. (B) Monthly change. (C) Ten-day change. (D) Daily change.

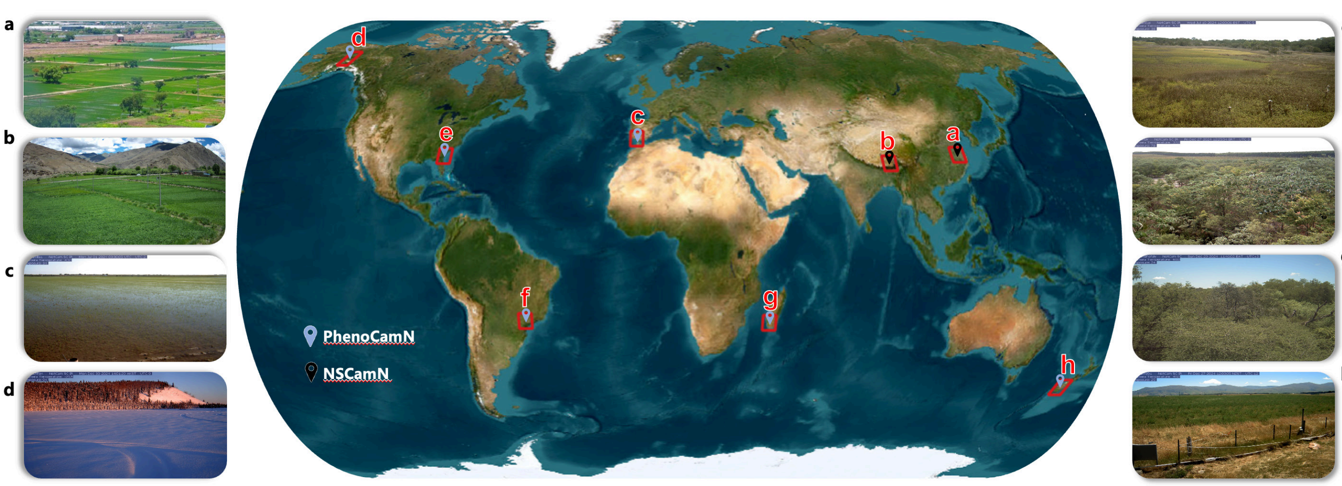

Fig. 3. Distribution of study area (eight 5° × 5° grids) and the images collected by near-surface cameras located in the center of Grid a to Grid h.

the tracking of intra-parcel spectral variations, providing a detailed view of daily land dynamics, such as crop rotations and vegetation changes. Together, these components create a robust and flexible workflow for multitemporal and multispatial land cover monitoring.

Annual land cover modification with near-surface cameras

The FGP 3.0 framework integrates multimodal remote sensing data, including multispectral imagery, SAR, and near-surface camera observations. Each of these data sources contributes

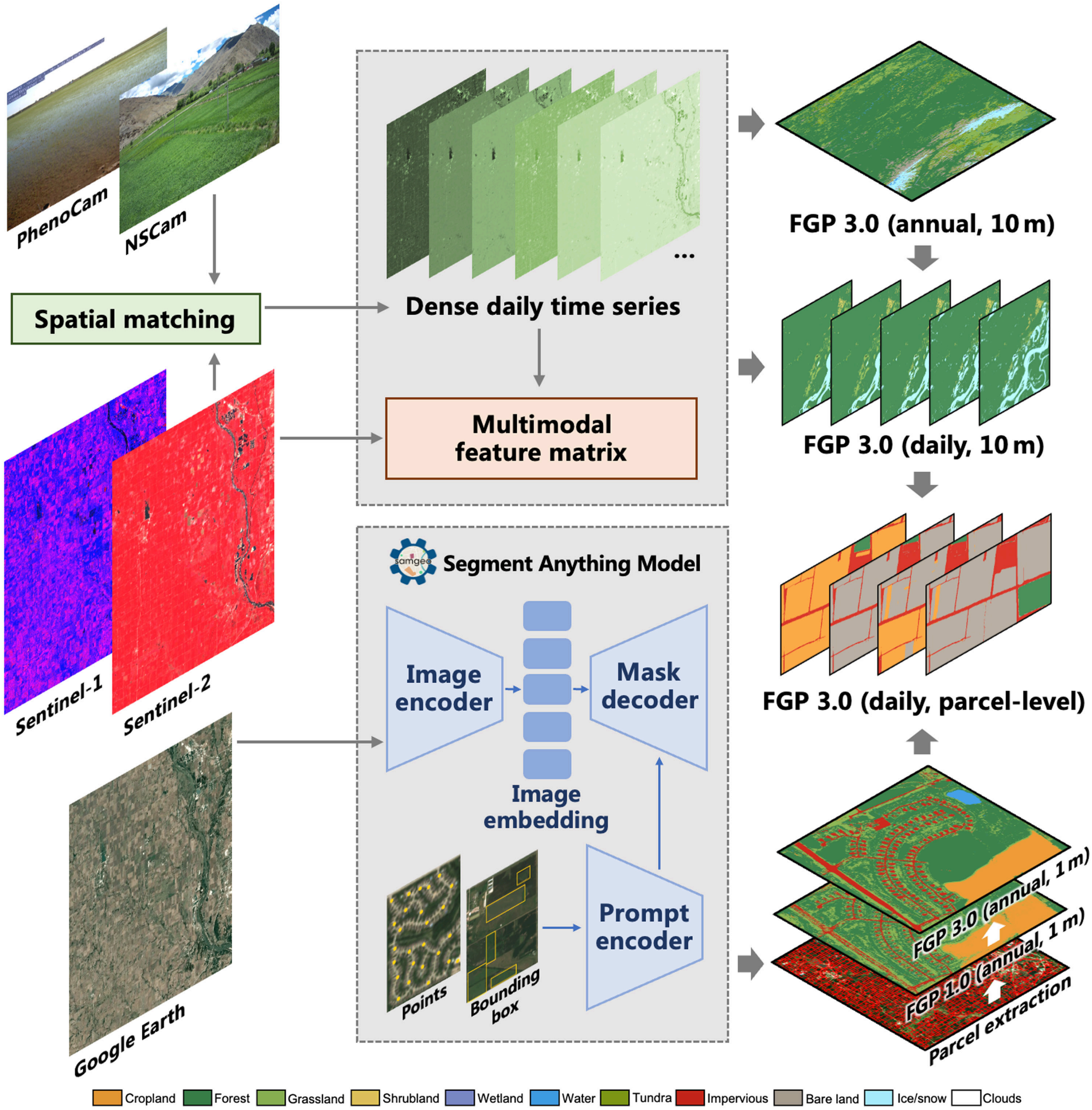

Fig. 4. The workflow of in-time land cover change mapping with multimodal data, dense surface observations, and SAM (FGP 3.0).

unique advantages to land cover classification to improve the mapping accuracy [64–66]. SAR data advantages include the ability to penetrate clouds and operate in all weather conditions, which is particularly beneficial for areas with frequent cloud cover or adverse weather [67–70]. Furthermore, SAR provides information on surface texture, moisture content, and structure, which enhances the discrimination of land cover types, especially in complex landscapes such as wetlands, urban areas, and agricultural fields [71–73]. Combining these capabilities with optical data further enriches the feature space for classification. Near-surface cameras complement satellite data by providing dynamic monitoring of surface conditions at an hourly or even sub-hourly intervals. These observations help fill data gaps caused by cloud cover, rain, or satellite revisit limitations, thereby enabling the construction of denser and more temporally continuous observation time series.

However, integrating near-surface camera imagery with satellite remote sensing data presents 2 main challenges: (a) the difference in imaging perspectives, as near-surface cameras capture oblique views compared to the perspective of satellite imagery, complicating spatial correspondence. (b) The limited spatial coverage of near-surface cameras, which provides point-based observations rather than regional-scale information, makes it challenging to scale observations from individual points to larger areas. To address these challenges, the study designed a series of algorithms to enable the application of near-surface camera data in annual land cover mapping.

First, an automated spatial matching algorithm was developed to align near-surface camera imagery with satellite data [42]. The near-surface camera images were divided into a grid of 10 × 10 cells, and for each grid cell, the 90th percentile of daily green chromatic coordinate (GCC) values was calculated, with the mean of these percentiles representing the daily GCC observation for the grid. A daily GCC time series was then constructed for each grid. Based on the approximate observation range of the camera, a set of random sampling points was selected within the range, and the annual NDVI time series from Sentinel-2 imagery was extracted for each sampling point. A linear regression analysis was performed between the NDVI time series of each sampling point and the GCC time series of various grid cells, and the grid with the smallest R^2 value was selected as the spatial match. Using the regression results, a functional relationship between GCC and NDVI was established, enabling the reconstruction of dense daily NDVI time series that integrate near-surface camera observations.

The point-based NDVI reconstruction was further extended to the entire study area by leveraging the first law of geography, which asserts spatial correlation. NDVI time series for all pixels in the study area were constructed based on the linear regression between the NDVI time series of sampling points and those of other pixels in the Sentinel-2 imagery. For dates with valid NDVI observations in each study area pixel, the original pixel values were retained, while missing NDVI values for other dates were supplemented using the results of the linear regression. This allowed the relationships between study area pixels (partially observed time series) and sampling points (fully observed time series) to be established, enabling the extrapolation of dense daily NDVI observations from sampling points to the entire study region. The reconstructed NDVI time series from near-surface cameras, combined with Sentinel-2 multispectral features and Sentinel-1 SAR features [VV (vertical/vertical) + VH (vertical/horizontal) polarization], formed the basis for land cover classification using a Random Forest classifier. Features used for classification included annual time series normalized burn ratio (NBR), normalized difference built-up index (NDBI), modified normalized difference water index (MNDWI), and annual time series Sentinel-1 backscattering coefficients. The temporal percentiles derived from the time series features were used for classification input to improve the accuracy and robustness of annual land cover mapping, and the multimodal temporal percentile matrix was derived by calculating percentiles (0th to 100th in 10% intervals) for each of the time series features stated above. The incorporation of dense annual time series allows for capturing seasonal and phenological variations across different land cover types, which enhances annual land cover classification accuracy [74]. Finally, the random forest classifier was selected due to its widespread use in large-scale land cover mapping, recognized for its strong generalization capability and reliable performance across diverse landscapes. For this study, one random forest classifier was trained for each of the 8 selected study regions, utilizing the enhanced time series features for robust and region-specific classification.

Dense dynamic land cover monitoring with near-surface cameras

With the increasing availability of near real-time satellite data, dynamic land cover monitoring has advanced considerably. Emerging products such as Google Dynamic World and FGP 2.0 provide near real-time dynamic monitoring capabilities. However, these products are constrained by satellite revisit frequencies and are susceptible to cloud and rain interference. As a result, their dynamic mapping is often limited to cloud-free imagery, leading to monitoring delays in highly cloudy or rainy regions. Moreover, abrupt or short-term land cover changes are frequently missed, making it difficult to achieve temporally continuous observations.

To address these limitations, this study leverages the sub-hourly dynamic monitoring capability of near-surface cameras and the reconstructed daily NDVI time series (see the previous section) to develop a method for daily dynamic land cover mapping. This method builds upon the dynamic mapping framework of FGP 2.0, incorporating the first all-season sample set (FAST) for daily sample migration and the updated annual land cover maps for the study area. For sample migration, the spectral angle distance (SAD) and Euclidean distance (ED) were calculated to measure the difference between the 2 spectral features in reference time and migration target time [25,75]. SAD was used to assess the shape variations between spectral vectors, while ED measured the absolute spectral difference in feature space. These 2 indicators were combined to identify the most spectrally similar samples, ensuring that migrated samples maintained consistency of the target period. Furthermore, the updated annual land cover maps were used as a reliable foundation for dynamic updates, as they are constructed using spectral and SAR features accumulated over an entire year, ensuring high accuracy and consistency [36]. Specifically, for the updated annual land cover maps, we also utilized the temporal percentile features derived from these annual time series to refine and update the classification results. Daily reconstructed imagery and migrated samples were then used to train a Random Forest classifier, which captures abrupt land cover changes and performs dynamic monitoring for each day. This combined approach—integrating dense daily observations with robust annual baselines—provides the necessary data support for identifying short-term land cover transitions and ensures continuity in daily dynamic land cover mapping. By addressing the limitations of satellite-based products, the proposed method establishes a robust framework for monitoring rapid and dynamic environmental changes in near real time.

High-resolution land cover map modification based on semantic segmentation

The FGP land cover mapping framework was designed with the primary objective of providing on-demand, multispatial, and multitemporal land cover products. In addition to supporting multitemporal land cover mapping (e.g., annual and dense dynamic mapping), FGP 3.0 extends its capabilities to optimize multispatial resolution land cover mapping. While FGP 1.0 relied on super-resolution post-processing to produce high-resolution (meter- and submeter level) land cover maps from 30-m/10-m datasets, a common challenge with high-resolution Google Earth remote sensing image classification is the occurrence of salt-and-pepper noise in the resulting maps [76]. To address this, FGP 3.0 explores a semantic segmentation-based approach for parcel-level high-resolution land cover mapping.

Specifically, FGP 3.0 leverages the SAM, a state-of-the-art computer vision model, through its application in remote sensing via the open-source tool Segment-Geospatial (samgeo) [77,78]. Samgeo, an extension of SAM tailored for geospatial data, facilitates automated parcel segmentation and object extraction from high-resolution remote sensing imagery. Based on SAM's prompt-based framework, samgeo enables object segmentation with minimal human supervision. This interactive segmentation approach provides flexibility and reduces the need for extensive labeled training datasets and additional model retraining. Without requiring additional sample annotation or model retraining, FGP 3.0 leverages the SAM model integrated within the samgeo framework to achieve automated parcel segmentation for high-resolution remote sensing imagery. To enhance the semantic information in SAM-generated segmentation results, we utilize the super-resolution results from FGP 1.0 as a reference for assigning land cover categories to the segmented parcels with a mode strategy. By integrating the interactive segmentation capabilities of SAM with the flexible geospatial segmentation framework provided by samgeo, FGP 3.0 offers a customizable and on-demand workflow for high-resolution land cover mapping. This process eliminates the need for extensive labeled datasets and bypasses the computational requirements of training deep learning models. It is also important to note that semantic information can be obtained from other publicly available land cover datasets. Additionally, for parcel-level dynamic mapping, the ground observations collected by NSCam can be integrated to enable dynamic classification and land cover allocation, further enhancing the accuracy and adaptability of the mapping process. Consequently, FGP 3.0 enables efficient, accurate, and scalable high-resolution land cover mapping, meeting the demands of diverse environmental and land management applications.

Results

Annual land cover map modification results

The experimental results comparing FGP 3.0 with other annual 10-m land cover mapping products highlight the improved performance of the proposed method in terms of overall mapping accuracy (Fig. 5). To evaluate the effectiveness of incorporating dense time series from near-surface cameras, we conducted a separate validation by removing the near-surface camera data, denoted as FGP 3.0*. Using 1,727 validation samples within the study area, FGP 3.0 achieved the highest average accuracy of 70.52%, followed by FGP 3.0* at 67.58%. The WorldCover and FROM-GLC products produced comparable accuracies of 65.72% and 64.13%, respectively. However, when examining accuracy across different grids, FROM-GLC exhibited a more consistent accuracy distribution, primarily between 60% and 70%, while WorldCover showed greater variability, with some grids achieving accuracies similar to FGP 3.0. The Dynamic World product, designed for dynamic land cover monitoring, demonstrated more pronounced variability across grids, with an average accuracy of approximately 55.72%, which may explain its limited performance in annual land cover mapping.

Furthermore, a notable outlier in the grid-based accuracy results (Fig. 5) is observed in a grid located in Europe (Grid c), where classification accuracy is obviously lower. Upon further analysis, this reduction in accuracy was attributed to confusion between cropland and shrubland. This issue is particularly pronounced in regions with Mediterranean climates, characterized by wet winters and dry summers. In these areas, coastal vegetation is predominantly shrubland, and agricultural fields are typically small and fragmented, interspersed with shrub cover, thereby increasing classification complexity. Additionally, the

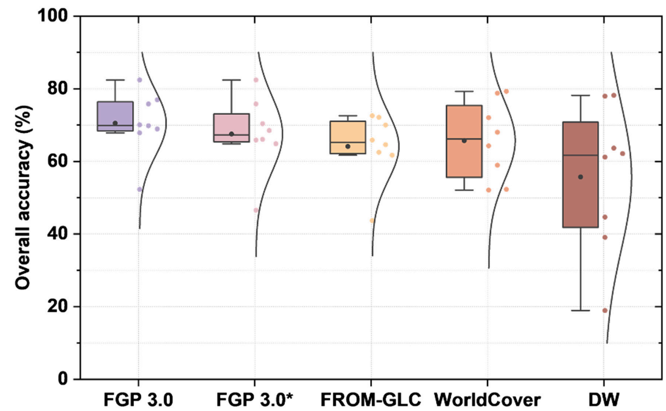

Fig. 5. The annual land cover overall accuracy distribution among the grids of the study area. DW, Dynamic World.

widespread practice of crop rotation and fallowing in this region often leads to fallow land being rapidly colonized by shrubs or weeds, further exacerbating confusion between cropland and natural shrubland. The integration of dense time series from near-surface cameras partially alleviates this issue. Compared to FGP 3.0*, the F1 score for cropland and shrubland of FGP 3.0 improved by 8.04% and 14.29%, respectively, when near-surface camera data were included. However, the misclassification between cropland and shrubland remains a significant challenge in these areas. This is primarily due to the limited spatial coverage of near-surface cameras, as the cameras deployed within the grid were positioned in relatively homogeneous, continuous cropland areas. We hypothesize that expanding the deployment of near-surface cameras to cover regions with interspersed cropland and shrubland along coastal zones could further enhance classification accuracy in these areas.

Based on the land cover maps of the grids of the study area presented in Fig. 6, FGP 3.0 effectively identifies complex land cover types, such as mixed vegetation zones, transitional urban–rural areas, and regions with seasonal variability. The inclusion of near-surface camera data enables FGP 3.0 to reconstruct daily time series, which complements the limitations of satellite observations caused by cloud cover or revisit intervals. The comparison between FGP 3.0 and FGP 3.0* (which excludes near-surface camera data) demonstrates the added value of these dense temporal observations. The results indicate that near-surface cameras contribute to the more accurate mapping of vegetation cover, such as the confusion among grassland, shrubland, and bare land (Fig. 6C and H), and the distinction between grassland and cropland in mixed agriculture–pastoral zones (Fig. 6G).

Dense dynamic land cover change monitoring results

The dense monitoring results presented in Fig. 7 demonstrate the effectiveness of the proposed method in capturing abrupt land cover changes on a daily basis across 2 distinct scenarios and regions. The first example (Fig. 7A) is derived from a near-surface camera station located in northern North America, with monitoring conducted from 2024 October 14 to 18. This example illustrates snow-induced land cover transitions, where previously exposed vegetation was progressively covered by snow over the observation period. The second example (Fig. 7B) corresponds to a near-surface camera station in southern Europe, with

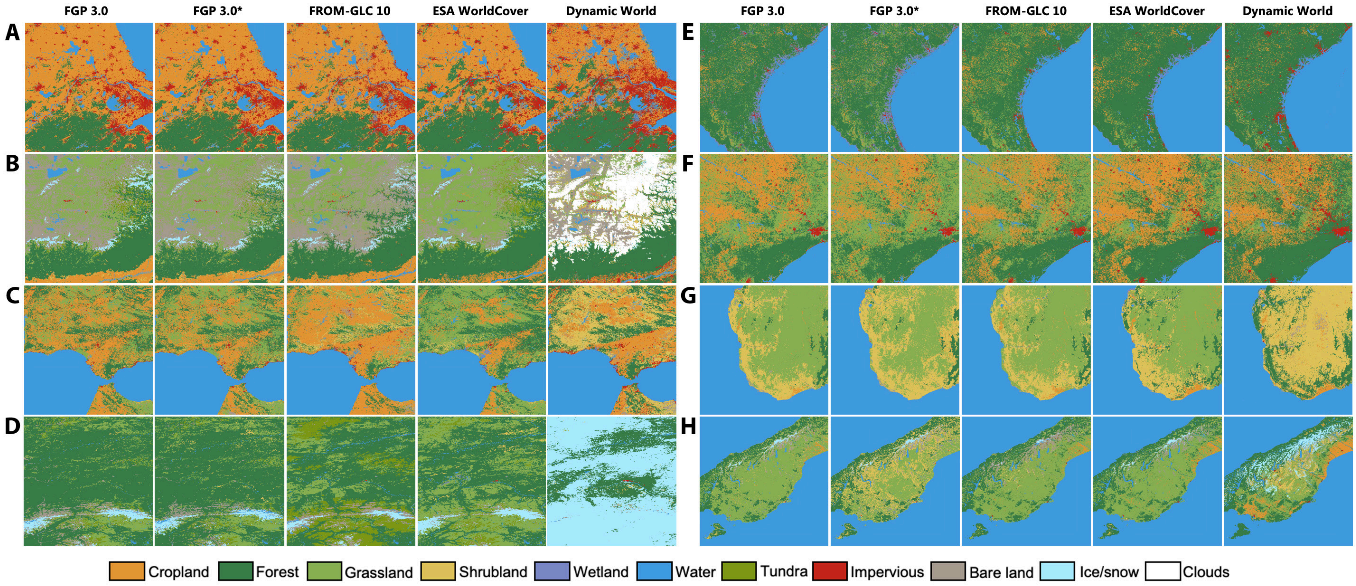

Fig. 6. The annual land cover mapping results of the grids compared to other 10-m global land cover products. (A to H) Eight study grids, which represent diverse terrestrial ecosystems as shown in Fig. 3.

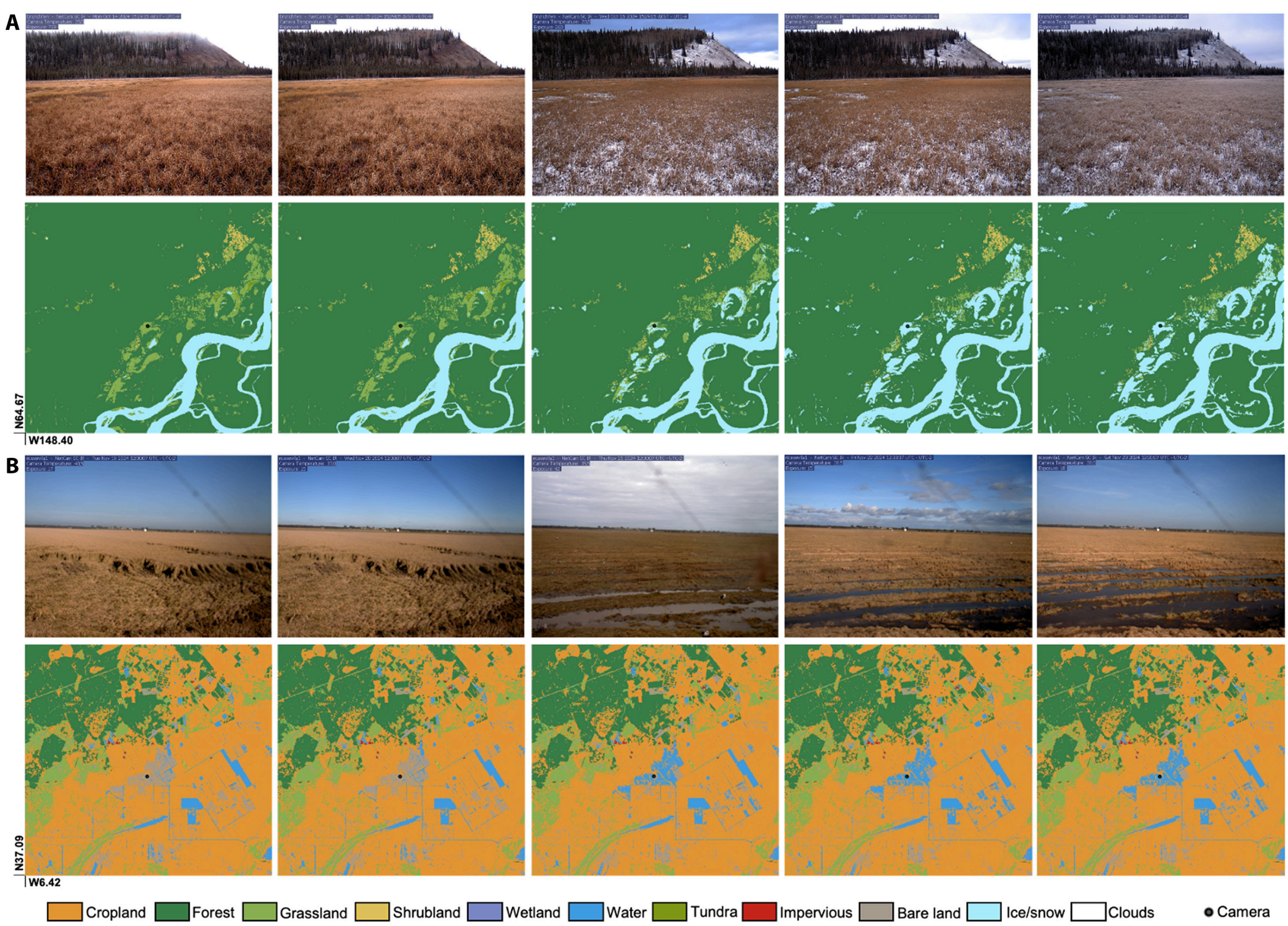

Fig. 7. The daily dynamic land cover change monitoring results located in (A) land cover dynamics caused by the snow in northern North America from 2024 October 14 to 18 and (B) land cover dynamics caused by the water expansion in south Europe from 2024 November 19 to 23.

monitoring carried out from 2024 November 19 to 23. This case highlights wetland dynamics caused by rising water levels, where previously exposed vegetation and bare soil were gradually inundated. These results underscore the capacity of the proposed method to monitor short-term dynamic land cover changes, which are often overlooked by existing dynamic products such as Google Dynamic World and FGP 2.0. Both products rely heavily on Sentinel-2 imagery and were unable to capture the changes shown in the 2 examples due to the lack of cloud-free Sentinel-2 observations during the specified time periods. The dependency on intermittent satellite data constrains their ability to detect short-lived or abrupt transitions, particularly in regions with frequent cloud cover or precipitation.

By leveraging reconstructed dense daily observations from near-surface cameras, the proposed method addresses these limitations. For the snow-induced transition in northern North America, the near-surface camera data provided continuous, high-temporal resolution monitoring that allowed for the capture of the snow accumulation process. Similarly, in southern Europe, the near-surface cameras enabled the detection of wetland dynamics on a daily basis, capturing subtle yet significant changes in the spatial extent of water. The ability to achieve such detailed monitoring through the integration of near-surface cameras and reconstructed dense imagery establishes FGP 3.0 as a robust tool for continuous land cover monitoring. This approach offers a reliable solution for addressing the challenges posed by regions with frequent cloud cover or highly dynamic landscapes, providing critical insights for environmental and ecological research.

High-resolution land cover map modification results

High-resolution land cover classification often focuses on urban and rural scenarios, such as the extraction of building footprints and agricultural fields. To evaluate the performance of FGP 3.0, high-resolution remote sensing imagery from different rural and urban settings in the United States and China was selected for classification (Fig. 8). In terms of computational resources, the segmentation process using the SAM-based geosam model required approximately 1 h to process a 10 km × 10 km mapping area. The model was run on an NVIDIA A100 GPU with 40 GB of memory. These resource requirements highlight the feasibility of implementing SAM for high-resolution land cover mapping to extend the approach to larger regions efficiently. The results highlight the strengths of the proposed FGP 3.0 framework in improving high-resolution land cover classification through parcel-level segmentation using the SAM. Compared with FGP 1.0 [25] and other high-resolution land cover products such as MULC [24] in the United States and SinoLC-1 in China [23], FGP 3.0 demonstrates notable advancements in both spatial accuracy and classification quality. The integration of SAM within the samgeo framework enables more cohesive and spatially consistent parcel-based classifications, addressing the common issue of salt-and-pepper noise that is faced with high-resolution remote sensing products of FGP 1.0. This improvement is evident in rural (Fig. 8A and C) and urban (Fig. 8B and D) areas, where the classification results produced by FGP 3.0 are cleaner and more homogeneous.

A key advantage of FGP 3.0 lies in its ability to accurately delineate the boundaries of different land cover features, such as water bodies, croplands, and urban structures. The segmentation approach ensures precise edge delineation, reducing misclassifications at feature boundaries, especially in areas where land cover types are spatially intertwined. For example, the water bodies and buildings in the urban and rural areas depicted in Fig. 8 are outlined with much greater precision than in FGP 1.0, MULC, and SinoLC-1, reflecting the enhanced edge detection capabilities of the SAM-based segmentation framework. Furthermore, FGP 3.0 mitigates the issue of shadow-induced misclassification, where shadows cast by tall buildings are often mistakenly classified as water bodies (Fig. 8B). However, the classification results of FGP 3.0 are fundamentally dependent on the super-resolution outputs from FGP 1.0. As a result, inaccuracies or errors present in the FGP 1.0 outputs may propagate into the FGP 3.0 results, limiting the overall accuracy of the final land cover classifications, such as the omission of water shown in Fig. 8A. Furthermore, although FGP 3.0 shows notable improvements in delineating individual land cover features, the SAM model exhibits limitations in effectively perceiving and segmenting background information. This shortcoming reduces its effectiveness in areas characterized by highly complex or heterogeneous land cover patterns, suggesting that further refinements are needed to accurately capture the detailed structure and variability of such landscapes. Nevertheless, the integration of SAM within the FGP 3.0 framework provides a flexible and efficient approach to high-resolution land cover classification. It is particularly advantageous for addressing common tasks such as building or field extraction, where precise segmentation and efficient processing are critical.

Furthermore, we combined the dense observations of near-surface cameras and land parcels obtained from SAM to provide parcel-level land dynamics (Fig. 9). This approach is particularly effective for monitoring cropland parcels [79], as high-resolution imagery provides accurate parcel boundary delineation, while the integration of Sentinel-2 imagery with NSCam observations enables the extraction of high-temporal resolution spectral information. For Fig. 9, the parcel segmentation results derived from Google Earth high-resolution imagery are overlaid onto Sentinel-2 imagery in the top row. This process highlights how parcel-level segmentation can produce more structured and organized land cover classification results, which avoids the fragmentation or misclassification that often occurs with pixel-based methods. Combined with Sentinel-2 and near-surface dense observations, the daily spectral variations within individual parcels can provide insights into crop dynamics at the field level. As shown in Fig. 9, the near-surface camera located in Henan, China captures the rotation of crops within the monitored parcels, which illustrates a typical crop rotation pattern of winter wheat followed by maize. This rotation is clearly captured through the combination of parcel-level segmentation and daily spectral observations, providing valuable data for agricultural monitoring and land management.

Discussion

This study presents a novel framework FGP 3.0 for land cover mapping by integrating near-surface camera images with satellite remote sensing data, demonstrating improvements in both annual and dynamic land cover monitoring with multiple temporal and spatial resolutions. The proposed approach leverages the continuous observation capabilities of NSCam to reconstruct dense daily time series and incorporates advanced deep learning models for high-resolution semantic segmentation.

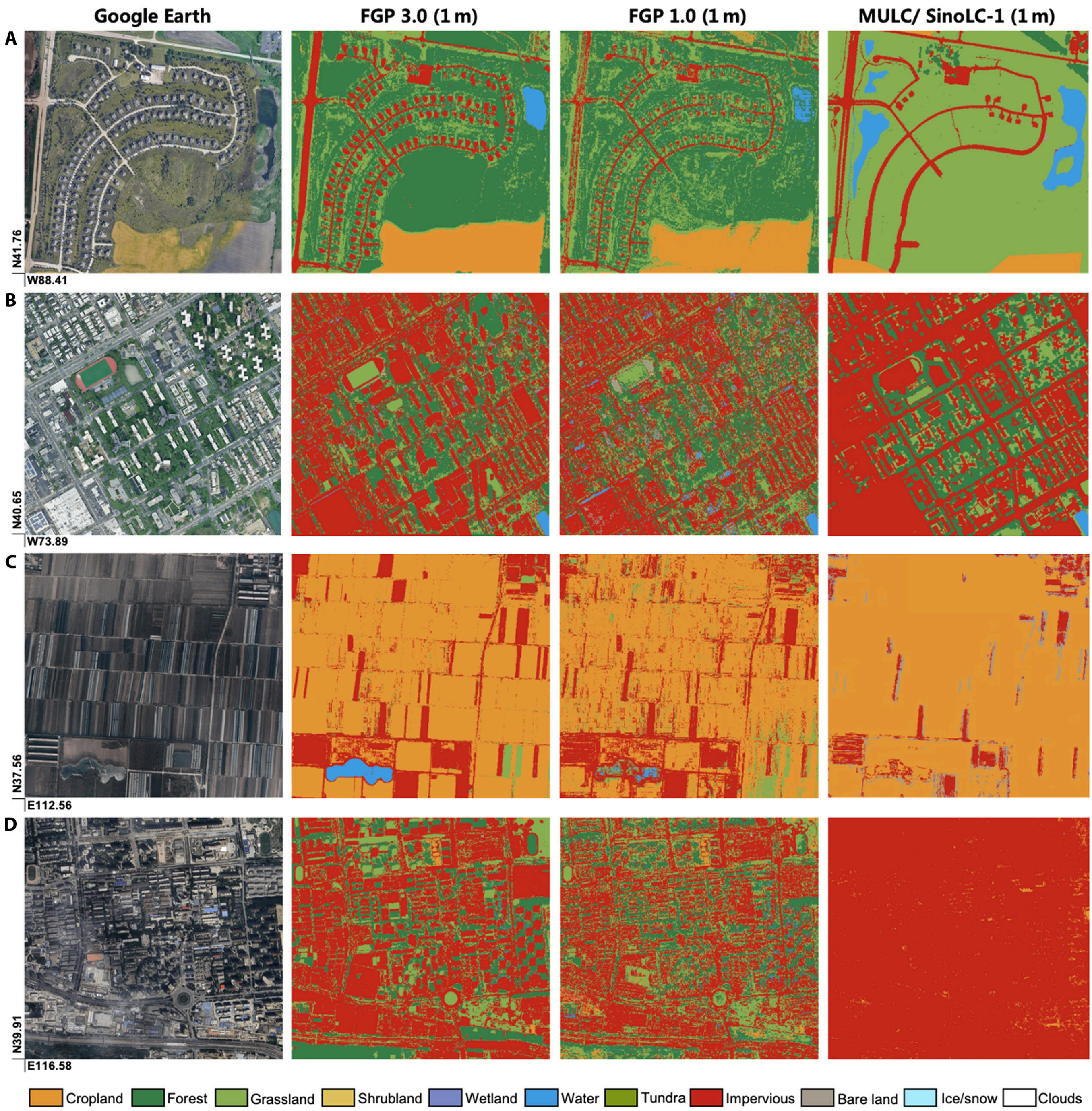

Fig. 8. The high spatial resolution land cover mapping results compared to FGP 1.0, MULC in the United States, and SinoLC-1 in China for (A) rural in the United States, (B) urban in the United States, (C) rural in China, and (D) urban in China.

The results present the potential of near-surface cameras for capturing fine-scale temporal and spatial land cover changes, particularly in regions with frequent cloud cover or rapid land cover changes. This section explores potential expansions and modifications of NSCamN, its applicability in validating existing dynamic land cover products, its potential for land system monitoring, and directions for future research.

Expansions and modifications of NSCamN

The deployment of NSCamN in real-world environments presents several significant challenges, particularly due to complex field factors such as insufficient site distribution, signal reception, and camera angle flexibility. Here, we discuss several solutions to effectively address the above challenges, which include appending supplementary field photographs and street view networks, improving signal reception capabilities, and designing a more flexible and controllable mechanism to adjust camera angles, leading to a more robust and comprehensive monitoring system.

First, augmenting NSCam network cameras with supplementary field photographs, captured by deploying additional lower-cost cameras or mobile devices, can enhance surface observation coverage, providing a more comprehensive view

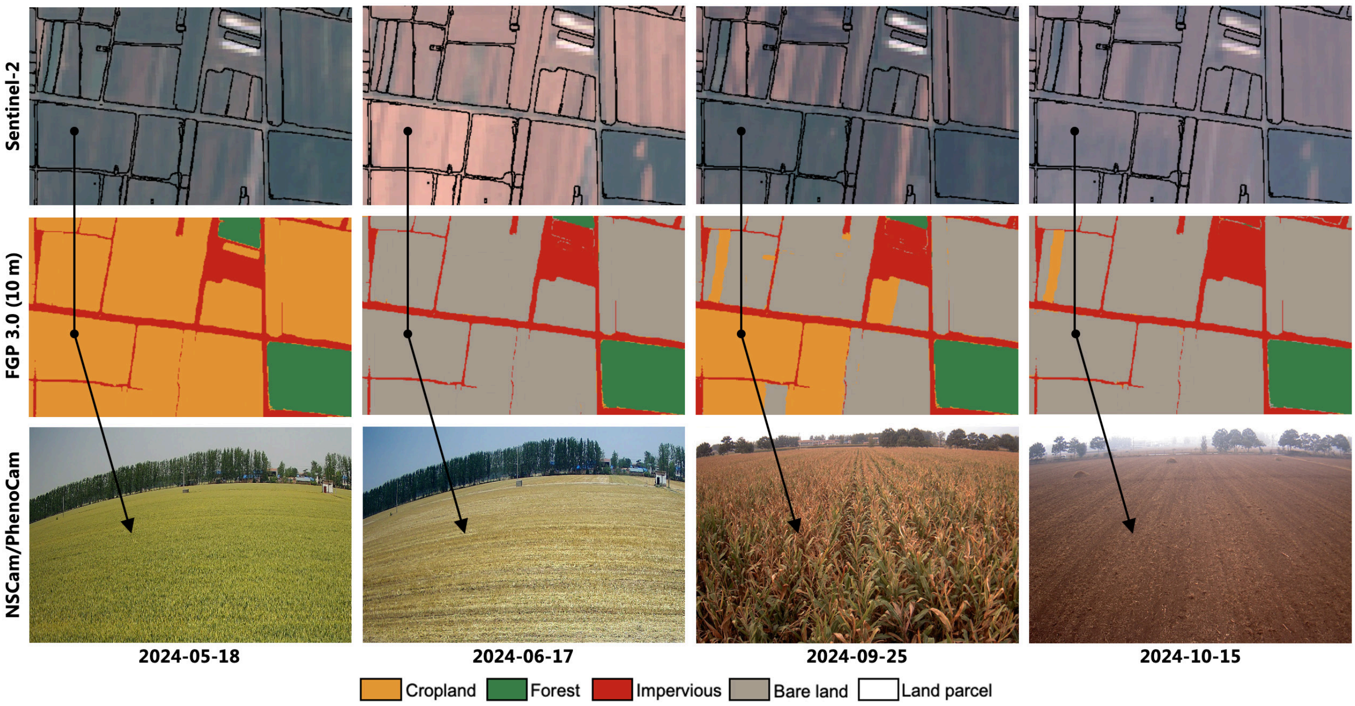

Fig. 9. Parcel-level land dynamic monitoring using the combination of near-surface camera dense observations at the site of Henan, China.

of the monitored area. Here, we collected the locations of main field photo networks around the globe, including the Global Geo-Referenced Field Photo Library [48], Land Use/Cover Area frame Survey (LUCAS, in Europe) [80], and USGS Land Cover Trends Dataset (in the USA) [81]. These field photo networks provide valuable supplement for phenology camera networks. Meanwhile, global street view networks also serve as valuable field photo data sources for validating land cover and land use changes. These networks provide billions of images worldwide through services like Google Street View and Baidu Street View and crowdsourcing platforms like Mapillary and KartaView. New datasets like Global Streetscapes offer a collection of 10 million crowdsourced street view images from 688 cities across 210 countries, enriched with over 300 attributes, addressing the gap of lacking comprehensive metadata [82], which enables further analysis and application of street view data source.

To evaluate the capability of matching single-time photos from noncontinuous near-surface cameras with satellite remote sensing imagery, we further analyzed photos taken by mobile cameras in Beijing. The results indicate that the majority of photos could be matched with satellite imagery within a time difference of 0 or 1 d, accounting for over 85% of the cases. Among these, 34.51% of the photos can be successfully matched with satellite data captured on the same day. For most of the remaining photos, the time difference for matching did not exceed 2 d (Fig. 10). These findings demonstrate the potential of integrating diverse data sources into NSCam network, such as global field photos and street views, to enhance the accuracy and comprehensiveness of land dynamics [83,84]. Moreover, mobile cameras and street view data offer additional opportunities for enriching land cover validation [85,86]. Recent advancements in machine learning and computer vision, including scene understanding algorithms, enable the automated interpretation of these photo-based datasets [87,88], which would be especially beneficial for capturing abrupt land cover changes or validating temporal land cover transitions in underrepresented regions, thereby addressing the gaps in traditional validation workflows.

Additionally, maintaining reliable signal reception in environments where terrain, vegetation, and urban structures can obstruct pathways is a major issue; for instance, 4G or 5G signals, commonly used for data transmission, can be significantly weakened in densely forested areas or wild areas. To address these issues, integrating external antennas and advancements in signal amplification technology are proposed for NSCam network to enhance the reliability of data transmission. Specifically, high-gain directional antennas can be deployed to extend communication range, while low-noise amplifiers (LNAs) and signal repeaters can help strengthen weak signals in challenging environments. Last but not least, achieving the desired camera angles for optimal coverage and observation is crucial. Fixed-angle cameras are limiting as they do not allow for adjustments to accommodate changing conditions or specific monitoring requirements. The design and implementation progress of pan–tilt–zoom (PTZ) mechanisms in NSCam cameras can significantly improve their flexibility and control, allowing for remote adjustments of the camera's pan, tilt, and zoom functions. PTZ mechanisms enable remote adjustments of the camera's pan (horizontal movement), tilt (vertical movement), and zoom functions, allowing for adaptive repositioning to accommodate seasonal changes in vegetation, shifts in hydrological conditions, or sudden environmental disturbances. This capability will also be particularly beneficial in dynamic environments where observation requirements may change over time.

Expanding NSCam's role in multiscale land monitoring systems

Significant progress has been made in dynamic land cover monitoring with the development of products such as Google

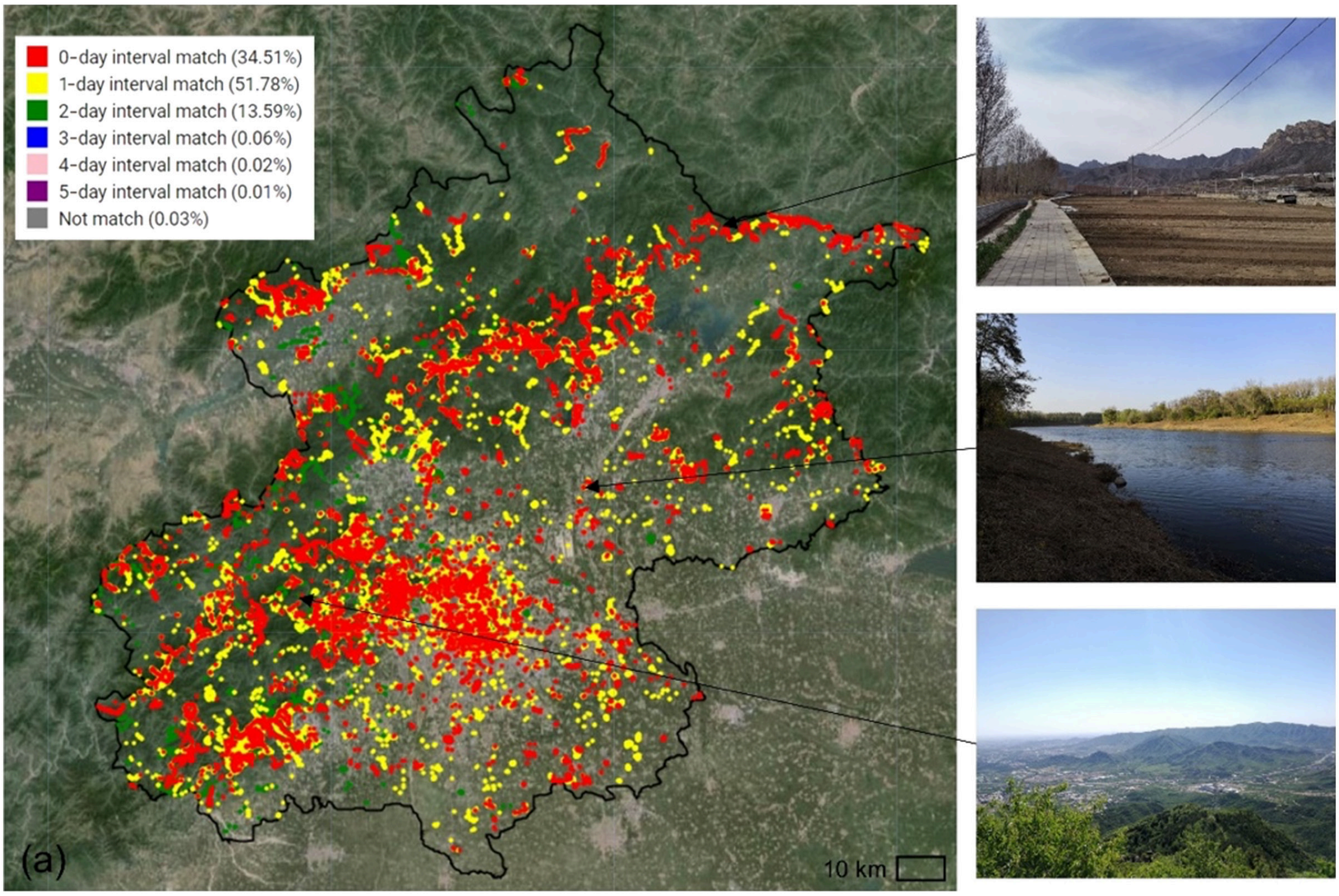

Fig. 10. Examples of supplementary field photographs enhancing observation coverage in Beijing, showing the differences in date between cameras and satellites (Landsat 8/9 and Sentinel-2).

Dynamic World and FGP, which leverage near real-time satellite data to capture land cover changes. The NSCam system, with its high temporal resolution and ground-level observations, provides more detailed phenological information for capturing surface changes. Therefore, for the classification system of dynamic land cover mapping, we can refine the existing standard land cover classification framework by incorporating phenological distinctions. For example, vegetation can be categorized into off-season and on-season, while croplands can be further divided into harvested farmland and actively growing cropland, depending on the land use status and seasonal phenological variations. These refinements would enhance the ability of dynamic land cover mapping to capture short-term transitions and agricultural cycles more accurately.

Furthermore, NSCam can serve as an independent and objective benchmark for evaluating the accuracy of these products. For instance, it can provide high-resolution validation data for abrupt land cover changes, such as snow cover dynamics or wetland expansion, as demonstrated in this study (Fig. 7). Such validation efforts not only improve the calibration and performance of dynamic mapping models but also enhance the reliability of real-time land cover monitoring for critical applications, including disaster response and ecosystem management. In addition, establishing a comprehensive near-surface camera network would facilitate the monitoring of land system changes, not only within a single year but also across multiyear time series. In this study, we combined PhenoCam site information with the FGP global land cover dataset to explore potential land system changes at these sites [25]. The results revealed that approximately 11% of PhenoCam sites exhibited potential land cover changes between 1982 and 2023. Among the unchanged sites, 44% are located in forested areas, 15% in croplands, and 11% in grasslands. Interestingly, these land cover types also constitute the primary categories involved in land cover changes. Specifically, 63% of the observed changes were driven by the conversion of cropland to grassland, while 17% resulted from the conversion of forest to grassland (Fig. 11A). Furthermore, about 11% of the sites showed evidence of potential urban expansion into cropland areas.

Beyond its role in product validation, a near-surface camera network holds considerable potential for monitoring land system degradation and broader environmental transformations. The fine temporal resolution of NSCam enables detailed tracking of critical indicators of land degradation, such as vegetation loss, hydrological shifts, and other ecosystem changes. These observations provide essential evidence for assessing the impacts of land use practices, climate change, and other anthropogenic activities on ecosystems. Specifically, NSCam facilitates high-frequency monitoring of land degradation processes, allowing for the detection of early signs of soil erosion, deforestation, and water stress. This capability is particularly critical in semi-arid and arid ecosystems, where vegetation cover

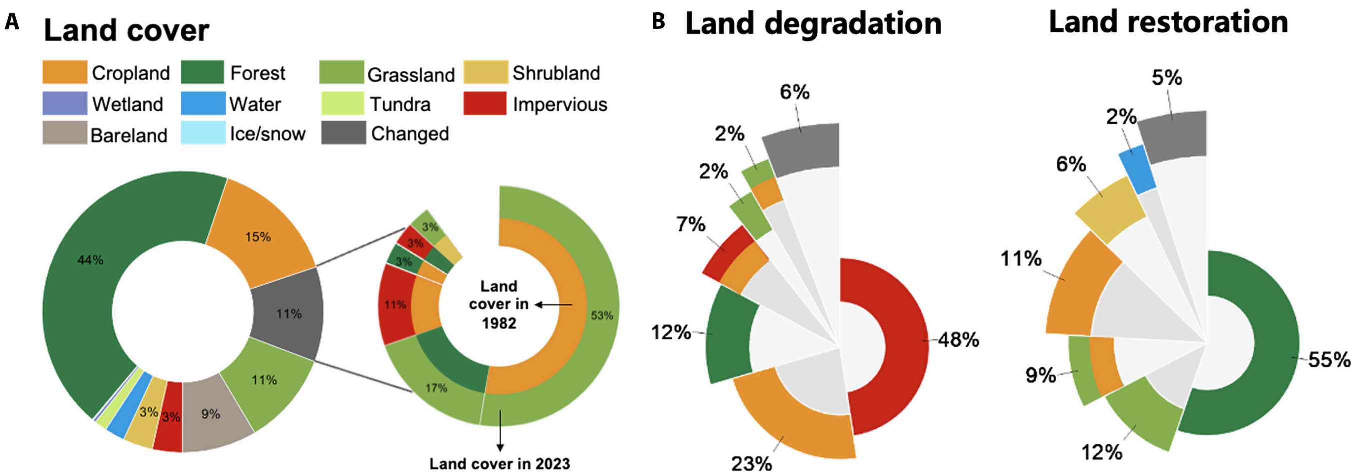

Fig. 11. Land system change of PhenoCam sites. (A) Land cover change during 1982–2023. (B) Land degradation and restoration during 2000–2023.

changes can serve as early warning signals for desertification risks. Additionally, NSCam enhances the ability to track hydrological variations, capturing seasonal fluctuations in water bodies and detecting prolonged drying trends in wetlands and rivers, which are crucial for managing water resources and mitigating the effects of droughts.

Moreover, early detection of ecosystem disturbances or land system changes enabled by NSCam could serve as a critical component of early warning systems, identifying emerging risks before they escalate into severe environmental crises. Current early warning systems primarily rely on meteorological data, but the dynamic land cover monitoring provided by NSCam offers a valuable complement [89,90]. For ecosystems and biodiversity, NSCam can track vegetation health and habitat changes, providing early alerts for deforestation or ecosystem degradation [91–93]. For geological hazards, it can detect shifts in vegetation cover or soil moisture, supporting landslide and erosion warnings [94,95]. For agriculture, it enables parcel-level monitoring of crop health and water stress, aiding in drought and pest warnings [42,96,97]. In urban areas, NSCam can monitor impervious surfaces and drainage changes, improving early detection of urban flooding and waterlogging risks [98–100].

To further explore these dynamics, we analyzed land degradation and restoration across PhenoCam sites since 2000 [101]. The results indicate that 33% of the sites exhibiting potential land degradation are located on impervious surfaces, followed by 28% in croplands and 18% in forested areas. In contrast, 59% of the sites displaying potential land restoration are located in forests (Fig. 11B). These findings highlight the potential of integrating NSCam into multiscale monitoring frameworks to better understand and validate land system changes and environmental challenges. By leveraging its fine temporal resolution and coupling it with global datasets, NSCam can provide critical insights into more informed land management and conservation strategies.

Conclusion

Timely land cover mapping is critical for monitoring environmental changes and supporting sustainable land management, yet challenges still remain in capturing abrupt and real-time land changes. This study introduces FGP 3.0, a framework that leverages multimodal datasets, including near-surface cameras, Sentinel-1 and Sentinel-2 imagery, and the high spatial resolution imagery along with the SAM foundation model to enhance multiple spatiotemporal land cover mapping. The results demonstrate that FGP 3.0 improves classification accuracy by reconstructing dense daily Sentinel-2 time series through the integration of near-surface cameras and satellite imagery. This approach also enables continuous and dense monitoring of land cover changes over time, offering valuable insights into rapid land transformations that are often missed by traditional satellite-based products. The integration of SAM further refines high spatial-resolution land cover classifications by delineating parcel boundaries, reducing salt-and-pepper noise, and improving edge accuracy for features like croplands, water bodies, and urban structures. Combined with high temporal-resolution remote sensing observations, this capability supports parcel-level dynamic monitoring, such as tracking crop rotation patterns in agricultural landscapes. The flexibility of FGP 3.0 positions it as a robust and scalable tool for multiscale and real-time land cover mapping. Its integration of high-frequency near-surface camera observations and multimodal datasets provides a foundation for implementing early warning systems to detect and address land system changes, as well as informing policy development and sustainable land management strategies.

Acknowledgments

We thank K. Jose from the Department of Humanities & Social Sciences, Birla Institute of Technology and Science, Pilani, for providing the locations of the Indian PhenoMet Network.
Funding: L.Y., X. Li, H.W., Q.Z., P.W., and Z.Z. were supported by the National Key R&D Program of China (2024YFF1307600). L.Y., X. Li, H.W., and Q.Z. were also supported by the Investigation Research Program between Ecological Environment and Human Health in Wuyi Mountain (20242120035), the open project of State Key Laboratory of Efficient Utilization of Arable Land in China, the Institute of Agricultural Resources and Regional Planning, Chinese Academy of Agricultural Sciences (No. EUAL-2025-03), the Chebaling National Nature Reserve Phenology Monitoring Network Construction and Application Project (CBLHT-2025050), the Xizang Science and Technology Plan Project (XZ202403ZY0018), and the National Key Scientific and Technological Infrastructure project "Earth System Science

Numerical Simulator Facility" (EarthLab). Z.D. was supported by the National Natural Science Foundation of China (42201367) and the Fundamental Research Funds for the Central Universities under grant DUT23RC(3)064.
Author contributions: L.Y. conceived the idea. Z.D. and L.Y. conducted the experiment. All authors provided resources, analyzed the results, and reviewed the manuscript.
Competing interests: The authors declare that they have no competing interests.

Data Availability

The data supporting the findings of this study are available at https://doi.org/10.6084/m9.figshare.29117393.

References

1. Chen X, Yu L, Du Z, Liu Z, Qi Y, Liu T, Gong P. Toward sustainable land use in China: A perspective on China's national land surveys. *Land Use Policy*. 2022;123:106428.
2. Yang J, Gong P, Fu R, Zhang M, Chen J, Liang S, Xu B, Shi J, Dickinson R. The role of satellite remote sensing in climate change studies. *Nat Clim Change*. 2013;3(10):875–883.
3. Zheng Z, Ma T, Roberts P, Li Z, Yue Y, Peng H, Huang K, Han Z, Wan Q, Zhang Y, et al. Anthropogenic impacts on Late Holocene land-cover change and floristic biodiversity loss in tropical southeastern Asia. *Proc Natl Acad Sci USA*. 2021;118(40):Article e2022210118.
4. Duveiller G, Caporaso L, Abad-Viñas R, Perugini L, Grassi G, Arneth A, Cescatti A. Local biophysical effects of land use and land cover change: Towards an assessment tool for policy makers. *Land Use Policy*. 2020;91:Article 104382.
5. Jiang L, Liu Y, Wu S, Yang C. Analyzing ecological environment change and associated driving factors in China based on NDVI time series data. *Ecol Indic*. 2021;129: Article 107933.
6. Morales C, Díaz ASP, Dionisio D, Guarnieri L, Marchi G, Maniatis D, Mollicone D. Earth Map: A novel tool for fast performance of advanced land monitoring and climate assessment. *J Remote Sens*. 2023;3:0003.
7. Brown CF, Brumby SP, Guzder-Williams B, Birch T, Hyde SB, Mazzariello J, Czerwinski W, Pasquarella VJ, Haertel R, Ilyushchenko S, et al. Dynamic world, near real-time global 10 m land use land cover mapping. *Sci Data*. 2022;9(1):251.
8. Li G, Fang C, Li Y, Wang Z, Sun S, He S, Qi W, Bao C, Ma H, Fan Y, et al. Global impacts of future urban expansion on terrestrial vertebrate diversity. *Nat Commun*. 2022;13(1):1628.
9. Wang Y, Sun Y, Cao X, Wang Y, Zhang W, Cheng X. A review of regional and global scale land use/land cover (LULC) mapping products generated from satellite remote sensing. *ISPRS J Photogramm Remote Sens*. 2023;206:311–334.
10. Liu LY, Zhang X, Gao Y, Chen XD, Shuai X, Mi J. Finer-resolution mapping of global land cover: Recent developments, consistency analysis, and prospects. *J Remote Sens*. 2021;2021:5289697.
11. Zhao T, Mu X, Song W, Liu Y, Xie Y, Zhong B, Xie D, Jiang L, Yan G. Mapping spatially seamless fractional vegetation cover over China at a 30-m resolution and semimonthly intervals in 2010–2020 based on Google Earth Engine. *J Remote Sens*. 2023;3:0101.
12. Phiri D, Simwanda M, Salekin S, Nyirenda VR, Murayama Y, Ranagalage M. Sentinel-2 data for land cover/use mapping: A review. *Remote Sens*. 2020;12(14):2291.
13. Wulder MA, Roy DP, Radeloff VC, Loveland TR, Anderson MC, Johnson DM, Healey S, Zhu Z, Scambos TA, Pahlevan N, et al. Fifty years of Landsat science and impacts. *Remote Sens Environ*. 2022;280:113195.
14. Sulla-Menashe D, Gray JM, Abercrombie SP, Friedl MA. Hierarchical mapping of annual global land cover 2001 to present: The MODIS Collection 6 Land Cover product. *Remote Sens Environ*. 2019;222:183–194.
15. ESA. Land cover CCI product user guide version 2.0 [Internet]. 2017. http://maps.elie.ucl.ac.be/CCI/viewer/download/ESACCI-LC-Ph2-PUGv2_2.0.pdf
16. Zhang X, Liu L, Chen X, Gao Y, Xie S, Mi J. GLC_FCS30: Global land-cover product with fine classification system at 30 m using time-series Landsat imagery. *Earth Syst Sci Data*. 2021;13(6):2753–2776.
17. Zhang X, Zhao T, Xu H, Liu W, Wang J, Chen X, Liu L. GLC_FCS30D: The first global 30 m land-cover dynamics monitoring product with a fine classification system for the period from 1985 to 2022 generated using dense-time-series Landsat imagery and the continuous change-detection method. *Earth Syst Sci Data*. 2024;16(3):1353–1381.
18. Chen J, Chen J, Liao A, Cao X, Chen L, Chen X, He C, Han G, Peng S, Lu M, et al. Global land cover mapping at 30 m resolution: A POK-based operational approach. *ISPRS J Photogramm Remote Sens*. 2015;103:7–27.
19. Gong P, Wang J, Yu L, Zhao Y, Zhao Y, Liang L, Niu Z, Huang X, Fu H, Liu S, et al. Finer resolution observation and monitoring of global land cover: First mapping results with Landsat TM and ETM+ data. *Int J Remote Sens*. 2013;34(7):2607–2654.
20. Zanaga D, Van De Kerchove R, Daems D, De Keersmaecker W, Brockmann C, Kirches G, Wevers J, Cartus O, Santoro M, Fritz S, Lesiv M, Herold M, Tsendbazar NE, Xu P, Ramoino F, Arino O. ESA WorldCover 10 m 2021 v200 [Internet]. Zenodo. 2022. [cited 2023 May 25] https://zenodo.org/record/7254221
21. Zanaga D, Van De Kerchove R, De Keersmaecker W, Souverijns N, Brockmann C, Quast R, Wevers J, Grosu A, Paccini A, Vergnaud S, Cartus O, Santoro M, Fritz S, Georgieva I, Lesiv M, Carter S, Herold M, Li L, Tsendbazar NE, Ramoino F, Arino O. ESA WorldCover 10 m 2020 v100 [Internet]. Zenodo. 2021 [cited 2023 May 25] https://zenodo.org/record/5571936
22. Gong P, Liu H, Zhang M, Li C, Wang J, Huang H, Clinton N, Ji L, Li W, Bai Y, et al. Stable classification with limited sample: Transferring a 30-m resolution sample set collected in 2015 to mapping 10-m resolution global land cover in 2017. *Sci Bull*. 2019;64(6):370–373.
23. Li Z, He W, Cheng M, Hu J, Yang G, Zhang H. SinoLC-1: The first 1 m resolution national-scale land-cover map of China created with a deep learning framework and open-access data. *Earth Syst Sci Data*. 2023;15(11):4749–4780.
24. Pilant A, Endres K, Rosenbaum D, Gundersen G. US EPA EnviroAtlas meter-scale urban land cover (MULC): 1-m pixel land cover class definitions and guidance. *Remote Sens*. 2020;12(12):1909.
25. Yu L, Du ZR, Dong RM, Zheng J, Tu Y, Chen X, Hao P, Zhong B, Peng D, Zhao J, et al. FROM-GLC Plus: Toward near real-time and multi-resolution land cover mapping. *Gisci Remote Sens*. 2022;59(1):1026–1047.
26. Wang L, Jiao W, MacBean N, Rulli MC, Manzoni S, Vico G, D'Odorico P. Dryland productivity under a changing climate. *Nat Clim Chang*. 2022;12(11):981–994.

27. Zhu Z, Qiu S, Ye S. Remote sensing of land change: A multifaceted perspective. *Remote Sens Environ*. 2022;282:113266.
28. McDowell NG, Allen CD, Anderson-Teixeira K, Aukema BH, Bond-Lamberty B, Chini L, Clark JS, Dietze M, Grossiord C, Hanbury-Brown A, et al. Pervasive shifts in forest dynamics in a changing world. *Science*. 2020;368(6494):Article eaaz9463.
29. Yang Y, Tilman D, Jin Z, Smith P, Barrett CB, Zhu YG, Burney J, Dodorico P, Fantke P, Fargione J, et al. Climate change exacerbates the environmental impacts of agriculture. *Science*. 2024;385(6713):Article eadn3747.
30. Zeng Y, Hao D, Huete A, Dechant B, Berry J, Chen JM, Joiner J, Frankenberg C, Bond-Lamberty B, Ryu Y, et al. Optical vegetation indices for monitoring terrestrial ecosystems globally. *Nat Rev Earth Environ*. 2022;3(7):477–493.
31. Boulton CA, Lenton TM, Boers N. Pronounced loss of Amazon rainforest resilience since the early 2000s. *Nat Clim Chang*. 2022;12(3):271–278.
32. Du Z, Yu L, Chen X, Li X, Peng D, Zheng S, Hao P, Yang J, Guo H, Gong P. An operational assessment framework for near real-time cropland dynamics: Toward sustainable cropland use in mid-spine belt of beautiful China. *J Remote Sens*. 2023;3:0065.
33. Liu Y, Ou C, Li Y, Zhang L, He J. Regularity of rural settlement changes driven by rapid urbanization in North China over the three decades. *Sci Bull*. 2023;68(18):2115–2124.
34. Song XP. The future of global land change monitoring. *Int J Digit Earth*. 2023;16(1):2279–2300.
35. Tian J, Zhu X, Shen M, Chen J, Cao R, Qiu Y, Xu YN. Effectiveness of spatiotemporal data fusion in fine-scale land surface phenology monitoring: A simulation study. *J Remote Sens*. 2024;4:0118.
36. Du Z, Yu L, Arvor D, Li X, Cao X, Zhong L, Zhao Q, Ma X, Wang H, Liu X, et al. Dual data- and knowledge-driven land cover mapping framework for monitoring annual and near-real-time changes. *IEEE Trans Geosci Remote Sens*. 2024;62:1–14.
37. Beamish A, Raynolds MK, Epstein H, Frost GV, Macander MJ, Bergstedt H, Bartsch A, Kruse S, Miles V, Tanis CM, et al. Recent trends and remaining challenges for optical remote sensing of Arctic tundra vegetation: A review and outlook. *Remote Sens Environ*. 2020;246:111872.
38. Zhu Z, Zhang J, Yang Z, Aljaddani AH, Cohen WB, Qiu S, Zhou C. Continuous monitoring of land disturbance based on Landsat time series. *Remote Sens Environ*. 2020;238:111116.
39. Moon M, Richardson AD, Friedl MA. Multiscale assessment of land surface phenology from harmonized Landsat 8 and Sentinel-2, PlanetScope, and PhenoCam imagery. *Remote Sens Environ*. 2021;266:112716.
40. Nijland W, Bolton DK, Coops NC, Stenhouse G. Imaging phenology; scaling from camera plots to landscapes. *Remote Sens Environ*. 2016;177:13–20.
41. Tran KH, Zhang X, Ketchpaw AR, Wang J, Ye Y, Shen Y. A novel algorithm for the generation of gap-free time series by fusing harmonized Landsat 8 and Sentinel-2 observations with PhenoCam time series for detecting land surface phenology. *Remote Sens Environ*. 2022;282:113275.
42. Yu L, Du Z, Li X, Zhao Q, Wu H, Weise D, Yuan X, Yang Y, Cai W, Song W, et al. Near surface camera informed agricultural land monitoring for climate smart agriculture. *Clim Smart Agric*. 2024;1(1):100008.
43. Bolton DK, Gray JM, Melaas EK, Moon M, Eklundh L, Friedl MA. Continental-scale land surface phenology from harmonized Landsat 8 and Sentinel-2 imagery. *Remote Sens Environ*. 2020;240:111685.
44. Ye Y, Zhang X, Shen Y, Wang J, Crimmins T, Scheifinger H. An optimal method for validating satellite-derived land surface phenology using in-situ observations from national phenology networks. *ISPRS J Photogramm Remote Sens*. 2022;194:74–90.
45. Yu L, Du Z, Li X, Zheng J, Zhao Q, Wu H, Weise D, Yang Y, Zhang Q, Li X, et al. Enhancing global agricultural monitoring system for climate-smart agriculture. *Clim Smart Agric*. 2025;2(1):100037.
46. Liu Y, Zhang X, Shen Y, Ye Y, Gao S, Tran KH. Evaluation of PlanetScope-detected plant-specific phenology using infrared-enabled PhenoCam observations in semi-arid ecosystems. *ISPRS J Photogramm Remote Sens*. 2024;210:242–259.
47. Nietupski TC, Kennedy RE, Temesgen H, Kerns BK. Spatiotemporal image fusion in Google Earth Engine for annual estimates of land surface phenology in a heterogenous landscape. *Int J Appl Earth Obs Geoinf*. 2021;99:102323.
48. Xu G, Zhu X, Fu D, Dong J, Xiao X. Automatic land cover classification of geo-tagged field photos by deep learning. *Environ Model Softw*. 2017;91:127–134.
49. Xu L, Ming D, Zhang L, Dong D, Qing Y, Yang J, Zhou C. Parcel level staple crop type identification based on newly defined red-edge vegetation indices and ORNN. *Comput Electron Agric*. 2023;211:108012.
50. Kirillov A, Mintun E, Ravi N, Mao H, Rolland C, Gustafson L, Xiao T, Whitehead S, Berg AC, Lo WY, Dollar P, Girshick R. Segment Anything. 2023 [cited 2025 Jan 5] https://openaccess.thecvf.com/content/ICCV2023/html/Kirillov_Segment_Anything_ICCV_2023_paper.html
51. Richardson AD, Hufkens K, Milliman T, Aubrecht DM, Chen M, Gray JM, Johnston MR, Keenan TF, Klosterman ST, Kosmala M, et al. Tracking vegetation phenology across diverse North American biomes using PhenoCam imagery. *Sci Data*. 2018;5(1):180028.
52. Seyednasrollah B, Young AM, Hufkens K, Milliman T, Friedl MA, Frolking S, Richardson AD. Tracking vegetation phenology across diverse biomes using version 2.0 of the PhenoCam dataset. *Sci Data*. 2019;6(1):222.
53. Wingate L, Ogée J, Cremonese E, Filippa G, Mizunuma T, Migliavacca M, Moisy C, Wilkinson M, Moureaux C, Wohlfahrt G, et al. Interpreting canopy development and physiology using a European phenology camera network at flux sites. *Biogeosciences*. 2015;12(20):5995–6015.
54. Moore CE, Brown T, Keenan TF, Duursma RA, van Dijk AIJM, Beringer J, Culvenor D, Evans B, Huete A, Hutley LB, et al. Reviews and syntheses: Australian vegetation phenology: New insights from satellite remote sensing and digital repeat photography. *Biogeosciences*. 2016;13(17):5085–5102.
55. Nasahara KN, Nagai S. Review: Development of an in situ observation network for terrestrial ecological remote sensing: The Phenological Eyes Network (PEN). *Ecol Res*. 2015;30(2):211–223.
56. Alberton B, Martin TCM, Da Rocha HR, Richardson AD, Moura MSB, Torres RS, Morellato LPC. Relationship between tropical leaf phenology and ecosystem productivity using phenocameras. *Front Environ Sci*. 2023;11:Article 1223219.
57. Alberton B, Torres RS, Cancian LF, Borges BD, Almeida J, Mariano GC, dos Santos J, Morellato LPC. Introducing digital cameras to monitor plant phenology in the tropics: Applications for conservation. *Perspect Ecol Conserv*. 2017;15(2):82–90.

58. Chandra S, Singh A, Mathew JR, Singh CP, Pandya MR, Bhattacharya BK, Solanki H, Nautiyal MC, Joshi R. Phenocam observed flowering anomaly of *Rhododendron arboreum* Sm. in Himalaya: A climate change impact perspective. *Environ Monit Assess*. 2022;194:877.
59. Jeganathan C, Singh B, Singh CP, Behera MD, Srivastava S, Natesha SR, Singh K, Ranjan R, Prakash M, Kumar A, et al. Integrated use of field sensors, PhenoCam, and satellite data for pheno-phase monitoring in a tropical deciduous forest of Dalma Wildlife Sanctuary, Jharkhand, India: Initial results from the Indian Phenology Network. *Conserv*. 2024;33: 3539–3565.
60. Jose K, Najeeb N, Bandopadhyay A, Singh CP, Chaturvedi RK. Unraveling meteorological drivers of leaf phenology in the Western Ghats, India. *Trees, Forests People*. 2025;20:100861.
61. Phadke DP, Chaurasia AN, Goroshi S, Ram M, Singh CP, Bhattacharya BK, Krishnayya NSR. Comparing two sensor data to perceive landscape phenology dynamics at Gir Wildlife Sanctuary, Gujarat, India. *Curr Sci*. 2024;127:1357–1362.
62. Sharma R, Kaur S, Uniyal SK. Tracking the seasonal dynamics of Himalayan birch using a time-lapse camera. *Folia Geobot*. 2021;56:125–138.
63. Keith DA, Ferrer-Paris JR, Nicholson E, Bishop MJ, Polidoro BA, Ramirez-Llodra E, Tozer MG, Nel JL, Mac Nally R, Gregr EJ, et al. A function-based typology for Earth's ecosystems. *Nature*. 2022;610(7932):513–518.
64. Chen L, Letu H, Fan M, Shang H, Tao J, Wu L, Zhang Y, Yu C, Gu J, Zhang N, Hong J, Wang Z, Zhang T. An introduction to the Chinese high-resolution Earth observation system: Gaofen-1~7 civilian satellites. *J. Remote Sens*. 2022.
65. Guo X, Lao J, Dang B, Zhang Y, Yu L, Ru L, Zhong L, Huang Z, Wu K, Hu D, He H, Wang J, Chen J, Yang M, Zhang Y, Li Y. SkySense: A multi-modal remote sensing foundation model towards universal interpretation for Earth observation imagery. 2024 [cited 2025 Jan 5] https://openaccess.thecvf.com/content/CVPR2024/html/Guo_SkySense_A_Multi-Modal_Remote_Sensing_Foundation_Model_Towards_Universal_Interpretation_CVPR_2024_paper.html
66. Kang W, Xiang Y, Wang F, You H. CFNet: A cross fusion network for joint land cover classification using optical and SAR images. *IEEE J Sel Top Appl Earth Obs Remote Sens*. 2022;15:1562–1574.
67. Bai Y, Sun G, Li Y, Ma P, Li G, Zhang Y. Comprehensively analyzing optical and polarimetric SAR features for land-use/land-cover classification and urban vegetation extraction in highly-dense urban area. *Int J Appl Earth Obs Geoinf*. 2021;103:102496.
68. Baier G, Deschemps A, Schmitt M, Yokoya N. Synthesizing optical and SAR imagery from land cover maps and auxiliary raster data. *IEEE Trans Geosci Remote Sens*. 2022;60:1–12.
69. Geng J, Ma W, Jiang W. Causal intervention and parameter-free reasoning for few-shot SAR target recognition. *IEEE Trans Circuits Syst Video Technol*. 2024;34(12):12702–12714.
70. Yuan B, Yu G, Li X, Li L, Liu D, Guo J, Li Y. Reconstructing long-term synthetic aperture radar backscatter in urban domains using Landsat time series data: A case study of Jing–Jin–Ji region. *J Remote Sens*. 2024;4:0172.
71. Chen Y, Bruzzone L. Self-supervised SAR-optical data fusion of Sentinel-1/-2 images. *IEEE Trans Geosci Remote Sens*. 2022;60:1–11.
72. Hong D, Hu J, Yao J, Chanussot J, Zhu XX. Multimodal remote sensing benchmark datasets for land cover classification with a shared and specific feature learning model. *ISPRS J Photogramm Remote Sens*. 2021;178:68–80.
73. Huang Z, Dumitru CO, Pan Z, Lei B, Datcu M. Classification of large-scale high-resolution SAR images with deep transfer learning. *IEEE Geosci Remote Sens Lett*. 2021;18(1):107–111.
74. Liu H, Gong P, Wang J, Wang X, Ning G, Xu B. Production of global daily seamless data cubes and quantification of global land cover change from 1985 to 2020—iMap World 1.0. *Remote Sens Environ*. 2021;258:112364.
75. Huang H, Wang J, Liu C, Liang L, Li C, Gong P. The migration of training samples towards dynamic global land cover mapping. *ISPRS J Photogramm Remote Sens*. 2020;161:27–36.
76. Zhang T, Hu D, Wu C, Liu Y, Yang J, Tang K. Large-scale apple orchard mapping from multi-source data using the semantic segmentation model with image-to-image translation and transfer learning. *Comput Electron Agric*. 2023;213:108204.
77. Osco LP, Wu Q, de Lemos EL, Gonçalves WN, Ramos APM, Li J, Marcato J. The Segment Anything Model (SAM) for remote sensing applications: From zero to one shot. *Int J Appl Earth Obs Geoinf*. 2023;124:103540.
78. Wu Q, Osco LP. Samgeo: A Python package for segmenting geospatial data with the Segment Anything Model (SAM). *J Open Source Softw*. 2023;8(89):5663.
79. Xu L, Ming D, Du T, Chen Y, Dong D, Zhou C. Delineation of cultivated land parcels based on deep convolutional networks and geographical thematic scene division of remotely sensed images. *Comput Electron Agric*. 2022;192:106611.
80. Martinez-Sanchez L, See L, Yordanov M, Verhegghen A, Elvekjaer N, Muraro D, d'Andrimont R, van der Velde M. Automatic classification of land cover from LUCAS in-situ landscape photos using semantic segmentation and a Random Forest model. *Environ Model Softw*. 2024;172:105931.
81. Soulard CE, Acevedo W, Auch RF, Sohl TL, Drummond MA, Sleeter BM, Sorenson DG, Kambly S, Wilson TS, Taylor JL, et al. Land cover trends dataset, 1973–2000. *US Geol Surv Data Series*. 2014;884.
82. Hou Y, Quintana M, Khomiakov M, Yap W, Ouyang J, Ito K, Wang Z, Zhao T, Biljecki F. Global Streetscapes—A comprehensive dataset of 10 million street-level images across 688 cities for urban science and analytics. *ISPRS J Photogramm Remote Sens*. 2024;215:216–238.
83. Fang F, Zeng L, Li S, Zheng D, Zhang J, Liu Y, Wan B. Spatial context-aware method for urban land use classification using street view images. *ISPRS J Photogramm Remote Sens*. 2022;192:1–12.
84. Kang J, Körner M, Wang Y, Taubenböck H, Zhu XX. Building instance classification using street view images. *ISPRS J Photogramm Remote Sens*. 2018;145(Part A):44–59.
85. Biljecki F, Ito K. Street view imagery in urban analytics and GIS: A review. *Landsc Urban Plan*. 2021;215:104217.
86. Li X, Zhang C, Li W. Building block level urban land-use information retrieval based on Google Street View images. *GISci Remote Sens*. 2017;54(6):819–835.
87. Kim JH, Lee S, Hipp JR, Ki D. Decoding urban landscapes: Google street view and measurement sensitivity. *Comput Environ Urban Syst*. 2021;88:101626.
88. Muhammad K, Hussain T, Ullah H, Ser JD, Rezaei M, Kumar N, Hijji M, Bellavista P, de Albuquerque VHC. Vision-based semantic segmentation in scene understanding for autonomous driving: Recent achievements, challenges, and outlooks. *IEEE Trans Intell Transp Syst*. 2022;23(12): 22694–22715.

89. Harrison L, Landsfeld M, Husak G, Davenport F, Shukla S, Turner W, Peterson P, Funk C. Advancing early warning capabilities with CHIRPS-compatible NCEP GEFS precipitation forecasts. *Sci Data*. 2022;9(1):375.
90. Piadeh F, Behzadian K, Alani AM. A critical review of real-time modelling of flood forecasting in urban drainage systems. *J Hydrol*. 2022;607:127476.
91. Besson M, Alison J, Bjerge K, Gorochowski TE, Høye TT, Jucker T, Mann HMR, Clements CF. Towards the fully automated monitoring of ecological communities. *Ecol Lett*. 2022;25(12):2753–2775.
92. Bhagabati B, Sarma KK, Bora KC. An automated approach for human-animal conflict minimisation in Assam and protection of wildlife around the Kaziranga National Park using YOLO and SENet Attention Framework. *Eco Inform*. 2024;79:102398.
93. Dertien JS, Negi H, Dinerstein E, Krishnamurthy R, Negi HS, Gopal R, Gulick S, Pathak SK, Kapoor M, Yadav P, et al. Mitigating human–wildlife conflict and monitoring endangered tigers using a real-time camera-based alert system. *Bioscience*. 2023;73(10):748–757.
94. Liu Y, Li C, Zhang J. Research of automatic monitoring and early warning technology based on real-time image recognition in landslide monitoring. In: *Proceedings of the 2024 International Academic Conference on Edge Computing, Parallel and Distributed Computing*. New York (NY): Association for Computing Machinery; 2024. p. 220–225.
95. Ripepe M, Lacanna G. Volcano generated tsunami recorded in the near source. *Nat Commun*. 2024;15(1):1802.
96. Garcia-Sanchez AJ, Garcia-Sanchez F, Garcia-Haro J. Wireless sensor network deployment for integrating video-surveillance and data-monitoring in precision agriculture over distributed crops. *Comput Electron Agric*. 2011;75(2):288–303.
97. Li X, Hou B, Tang H, Talpur BA, Zeeshan Z, Bhatti UA, Liao J, Liu J, Alabdullah B, Naimi ISA. Abnormal crops image data acquisition strategy by exploiting edge intelligence and dynamic-static synergy in smart agriculture. *IEEE J Sel Top Appl Earth Obs Remote Sens*. 2024;17:12538–12553.
98. Kuglitsch MM, Cox J, Luterbacher J, Jamoussi B, Xoplaki E, Thummarukudy M, Radwan GS, Yasukawa S, McClain SN, Albayrak RA, et al. AI to the rescue: How to enhance disaster early warnings with tech tools. *Nature*. 2024;634(8032):27–29.
99. Lo SW, Wu JH, Chang JY, Tseng CH, Lin MW, Lin FP. Deep sensing of urban waterlogging. *IEEE Access*. 2021;9: 127185–127203.
100. Wang X, Wang M, Liu X, Zhu L, Glade T, Chen M, Zhao W, Xie Y. A novel quality control model of rainfall estimation with videos—A survey based on multi-surveillance cameras. *J Hydrol*. 2022;605:127312.
101. Du Z, Yu L, Chen X, Gao B, Yang J, Fu H, Gong P. Land use/cover and land degradation across the Eurasian steppe: Dynamics, patterns and driving factors. *Sci Total Environ*. 2024;909:168593.

Journal of Remote Sensing
A SCIENCE PARTNER JOURNAL

FROM-GLC Plus 3.0: Multimodal Land Change Mapping with SAM and Dense Surface Observations

Le Yu, Zhenrong Du, Xiyu Li, Jiatong Gu, Xinyue Li, Liheng Zhong, Duojiweise, Hui Wu, Qiang Zhao, Xiaorui Ma, Junqing Zheng, Yuanzheng Yang, Weimin Song, Pei Wang, Zhicong Zhao, Lingyun Liao, Ying Long, Yongguang Zhang, Jinbang Peng, Miaogen Shen, Tingting Li, Zhentao Sun, Yonggan Zhao, Chaoyang Wu, Guanghui Lin, Yong Luo, and Dailiang Peng

Citation: Yu L, Du Z, Li X, Gu J, Li X, Zhong L, Duojiweise, Wu H, Zhao Q, Ma X, et al. FROM-GLC Plus 3.0: Multimodal Land Change Mapping with SAM and Dense Surface Observations. *J Remote Sens*. 2025;**5**:0728. DOI: 10.34133/remotesensing.0728

Land cover mapping plays a critical role in monitoring land system changes. Despite advancements in remote sensing technologies, traditional satellite-based approaches are often constrained by cloud cover, coarse temporal resolution, and limitations in capturing fine-scale landscape dynamics, leading to gaps in continuous and real-time monitoring. Near-surface cameras offer a solution by providing high-frequency, ground-level observations that bridge temporal gaps and enhance spatial detail. Therefore, this study makes substantial contributions by pioneering the integration of near-surface camera observations with satellite imagery, addressing key challenges in imaging perspective differences and limited coverage of ground-based observations for enhanced land cover monitoring at a 30-m/10-m scale. A key innovation lies in leveraging near-surface cameras to reconstruct dense satellite data time series and capture daily land cover dynamics, addressing critical temporal gaps in traditional satellite-based approaches. The research further advances the field by implementing state-of-the-art deep learning techniques, particularly the Segment Anything Model (SAM), to achieve precise parcel-level delineation and reduce classification noise at a high-resolution (meter- and submeter level) scale. Furthermore, the framework's ability to synthesize multimodal data sources (near-surface cameras, Sentinel-1/2, and high-resolution imagery) represents a methodological breakthrough in space and surface sensor integration for real-time land cover change detection, enabling time-sensitive applications and early warning systems for land system changes.
Image

Journal of Remote Sensing (ISSN 2694-1589) is published by the American Association for the Advancement of Science. 1200 New York Avenue NW, Washington, DC 20005.